10.2514/6.2025-2416

Flight Testing Instrumentation Development and Integration for a Subscale Integrated High Lift Propulsor Testbed

Or D. Dantsker* — *Indiana University, Bloomington, IN 47408*
Renato Mancuso† — *Boston University, Boston, MA 02215*
Byron Ward‡ and Christian Miller§ — *Wayfarer Aircraft Research & Development, La Mesa, CA 91941*
Donovan Shea¶ and Kyle Collins‖ — *Embry Riddle Aeronautical University, Dayonta Beach, FL 32114*

Recent advancements in electric and hybrid-electric aircraft have sparked interest in Advanced Aerial Mobility (AAM), enabling innovative air transport solutions. Distributed Electric Propulsion (DEP), with its favorable aero-propulsive interactions, is a key focus for advanced aircraft designs, and thus an area of significant interest for academia and industry. Wayfarer Aircraft has developed and patented a novel new form of of blown wing lift augmentation called the Integrated High Lift Propulsor (IHLP), which uses DEP integrated with a Krueger slat or flap. This paper presents the instrumented, reconfigurable subscale IHLP distributed electric propulsion testbed that will be used to parameterize the performance and handling qualities (P&HQ) of IHLP. The subscale aircraft, which was developed from a 35%-scale Cessna 182 R/C scale model aircraft, was instrumented with a custom-integrated flight control and data acquisition system developed to enable this flight research — specifically a Holybro Pixhawk 6X autopilot running custom flight control software coupled with a custom version of the Al Volo FDAQ data acquisition system. The paper presents IHLP including its advantages and performance improvements in high-lift and cruise conditions compared to conventional distributed electric propulsion (DEP) systems. The detailed development of the IHLP subscale testbed are presented, including modifications, instrumentation design, and the integration of the data acquisition and flight control systems. Preliminary results from ground testing are presented to demonstrate the capabilities of the instrumented IHLP testbed.

Nomenclature

AAM	=	Advanced Aerial Mobility	*IMU*	=	Inertial Measurement Unit
ADC	=	Analog-to-Digital Converters	*I/O*	=	Input Output
AHRS	=	Attitude and Heading Reference System	*PCB*	=	Printed Circuit Board
CFD	=	Computational Fluid Dynamics	*PID*	=	Parameter IDentification
CPU	=	Central Processing Unit	*PTI*	=	Programmed Test Input
DEP	=	Distributed Electric Propulsion	*PPM*	=	Pulse Position Modulation
DOF	=	Degree of Freedom	*PWM*	=	Pulse Width Modulation
ESC	=	Electronic Speed Controller	*P&HQ*	=	Performance and Handling Qualities
GNSS	=	Global Navigation Satellite System	*R/C*	=	Radio Control
IC	=	Integrated Circuit	*RPM*	=	Revolutions Per Minute
IHLP	=	Integrated High Lift Propulsor	*SA*	=	Situational Awareness

*Assistant Professor, Department of Intelligent Systems Engineering. odantske@iu.edu. AIAA Member.
†Associate Professor, Department of Computer Science. rmancuso@bu.edu
‡CEO. byron@ward.aero. AIAA Member
§Engineer, Wayfarer Aircraft R&D. christian@ward.aero.
¶Graduate Research Assistant, Eagle Flight Research Center. shead5@my.erau.edu. AIAA Member
‖Director, Eagle Flight Research Center. collink9@erau.edu.

STC	=	Supplemental Type Certificate	$VTOL$	=	Vertical Takeoff and Landing
$STOL$	=	Short Takeoff and Landing			
UAV	=	Uncrewed Aerial Vehicle			
A_p	=	Propeller Disk Area	S_G	=	Takeoff Ground Distance
c	=	Wing Chord	Q	=	Torque
C_L	=	Lift Coefficient	T	=	Thrust
D	=	Propeller Diameter	W	=	Weight
L/D	=	Lift / Drag	α	=	Angle of Attack
q	=	Dynamic Pressure	β	=	Angle of Sideslip
S	=	Wing Area			

I. Introduction

Recent technical advancements and research have generated substantial interest in electric and hybrid-electric aircraft for Advanced Aerial Mobility (AAM), where transformative and disruptive new aircraft are used to transport people and things in new ways to new locations not served by current air transport. This market is expected to grow to $ 120 billion dollars in worldwide vehicle sales by 2030. Fueled by similar technological advancements, by 2030 the market for autonomous and remotely piloted aircraft used in military, public safety, agriculture, and enterprise is expected to grow to $ 90 billion dollars globally.

The favorable aero-propulsive interactions of Distributed Electric Propulsion (DEP) are a key enabling technology for many advanced configurations, and thus an area of significant interest for academia and industry. Use cases include increasing wing loading for cruise efficiency,[1–4] super Short Takeoff and Landing (STOL) aircraft,[5] tilt-wing and deflected slipstream Vertical Takeoff and Landing (VTOL) aircraft,[6–8] and even new wing-in-ground effect aircraft.[9]

Wayfarer Aircraft has developed and patented a novel new form of of blown wing lift augmentation called the Integrated High Lift Propulsor (IHLP), which uses DEP integrated with a Krueger slat or flap. A skematic of IHLP is shown in Fig. 1. The integrated system substantially reduces the thrust and power required for lift augmentation while stowing internally to increase cruise efficiency.

Wind tunnel testing was recently conducted at Mississippi State University's low speed wind tunnel to evaluate the performance of the IHLP.[10] Starting from a baseline configuration determined from pretest Computational Fluid Dynamics (CFD) analyses, a parametric study was performed to determine the influence on the aerodynamic characteristics. The study involved variations in flap settings, slat angles, overlap, propeller tilt, and propeller position. The

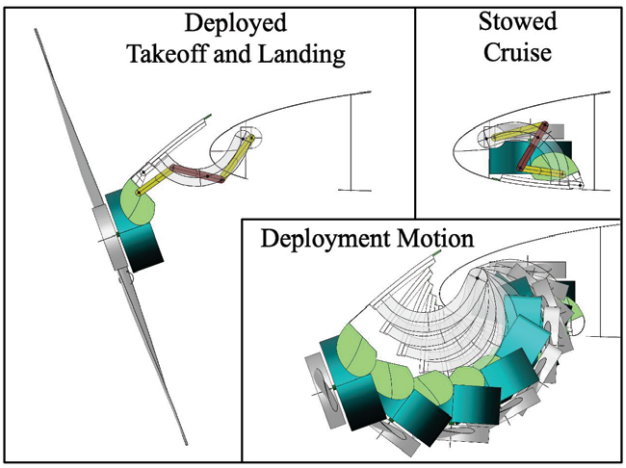

Figure 1. Schematic of the Integrated High Lift Propulsor.

impact of Reynolds number, propeller RPM, and the use of trips on system performance were also explored. Results confirmed the effectiveness of the IHLP in achieving high lift capabilities. The findings from the experimental work suggest the IHLP as a promising technology for advancing high lift capabilities in DEP systems.

To further validate the performance of IHLP, a reconfigurable subscale distributed electric propulsion testbed is under development. The testbed aircraft, based off a of a 35%-scale Cessna 182 scale radio control model aircraft, will provide full-scale representative flight test data. The aircraft Performance and Handling Qualities (P&HQ) will be first characterized in its baseline configuration with comparison to full-scale Cessna 182 flight test data. The aircraft will then be reconfigured to incorporate the IHLP using a rapidly reconfigurable installation with up to 12 DEP motors along the wing, in addition to the main tractor propeller of the baseline aircraft. Flight testing of the IHLP modified aircraft will establish the incremental P&HQ effect of the DEP. Concept images of the final aircraft instrumentation and flight controller operation are shown in Fig. 2. Flight testing will involve classic flight test maneuvers as well as manually automated maneuver injection for parameter identification (PID) of aircraft and IHLP performance. A custom-integrated flight control and data acquisition system had to be developed to enable this flight testing research — specifically a Holybro Pixhawk 6X autopilot running custom flight control software coupled with a custom version of the Al Volo FDAQ data acquisition system. Photos of these systems are shown in Fig. 3. The development and integration of this custom flight testing instrumentation for the IHLP reconfigurable distributed electric propulsion subscale testbed is the focus of this paper.

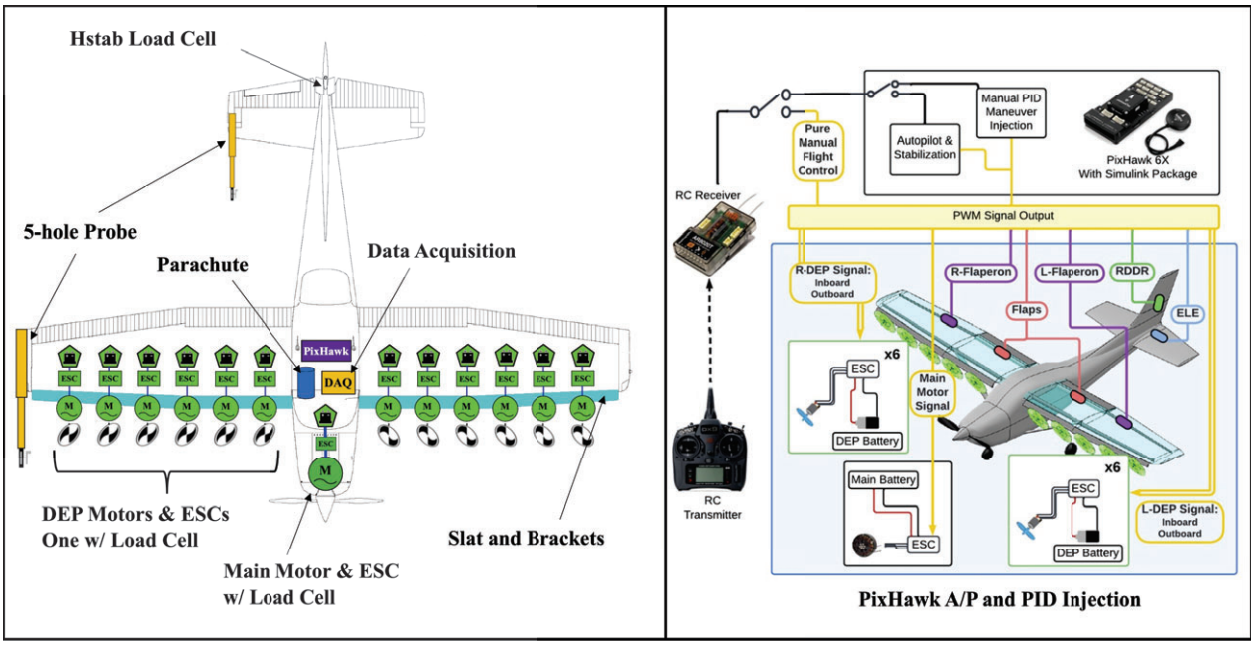

Figure 2. Concept images of the Integrated High Lift Propulsor Subscale Testbed.

(a) (b)

Figure 3. The (a) Holybro Pixhawk 6X (photo taken from Holybro) and (b) Al Volo FDAQ (photo taken from Al Volo).

Specifically, the paper is structured as follows: Section II describes the Integrated High Lift Propulsor including its benefits producing powered lift and impact on high lift and cruise conditions, compared to conventional DEP systems. Then, Section III introduces the IHLP reconfigurable distributed electric propulsion subscale testbed and the modifications that have been made to date. Afterwards, Section IV presents the design aspects involved in developing the instrumentation used on the IHLP subscale aircraft. Next, Section V describes how the instrumention, specifically the data acquisition system and the flight control system were developed. Section VI then presents the instrumentation integrated into the IHLP subscale testbed, and is followed by Section VII that presents the aircraft flight controls. Section VIII provides the results of preliminary ground testing of the aircraft. The paper concludes in Section IX with a summary and statement of future work.

II. Integrated High Lift Propulsor System

A. Introduction

The IHLP is a new form of powered or 'blown' lift, which uses favorable propeller-wing interactions to increase the lift capability ($C_{L,max}$) of a wing. While the general concept of powered lift has long been known, recent advances in battery and electric motor technology have made new configurations viable.

The IHLP uses DEP integrated with a Krueger flap or slat (Fig. 1). In the deployed position the slat serves as a structural mount for the propulsor, provides the traditional aerodynamic benefit, and has additional synergistic integration impact on propeller-wing interaction described subsequently. In the cruise configuration the propulsor is stored internally within the wing, with the slat serving as a door to cover the compartment as well as the mechanism to move the propulsor from the stowed to deployed position. The propulsor can be moved from the stowed to deployed position, as shown in Fig. 1, using mechanical linkages similar to in-service folding nose Krueger flaps. While conceptually and mechanically straightforward, this invention exploits complex propulsion-wing interactions to offer substantial aircraft level benefits, including substantially reduced power for a given $C_{L,max}$, more favorable propeller-motor matching for weight and cost efficiency, and a reduction in cruise drag by minimizing the high lift system impact to the cruise optimized wing shape. This increased efficiency significantly reduces the overall weight and cost impact of the high lift system, resulting in a lighter, cheaper, and more energy efficient aircraft.

B. Benefits of Powered Lift

The fundamental purpose of the IHLP is to improve the efficiency and commercial viability of powered or 'blown' lift, which uses favorable propeller-wing interactions to increase the high lift capability ($C_{L,max}$) of a wing. Increased high lift capability may be used to improve aircraft payload, field length, or cruise efficiency. From fundamental relationships, takeoff distance is a function of wing loading, thrust to weight, and maximum lift coefficient.

$$S_G \propto \left(\frac{1}{C_{L,LO}}\right)\left(\frac{W}{S}\right)\left(\frac{W}{T}\right) \tag{1}$$

Increasing lift coefficient allows some combination of wing loading increase for aerodynamic cruise efficiency, thrust to weight reduction for propulsive cruise efficiency ("power shaving"), or a shorter runway to be used. Reduced runway lengths enable more community-centric, optimally located airports providing an accessible and efficient mobility network.

The connection between $C_{L,max}$ improvement via DEP and power shaving has received less attention but takes on increasing importance as cruise efficiency is emphasized, increasing the mismatch between takeoff and cruise power. For example, the Green Flight Challenge winning Pipistrel Taurus 4 used five times the power for takeoff as for cruise[11] to meet the competition field length requirement. Similarly, in-service long endurance Unmanned Aerial Vehicles (UAVs) use low power loading for cruise efficiency, but are often required to operate from ships, semi-improved airfields, and austere locations. For multi-engine aircraft, the installed power is typically set by One Engine Inoperative (OEI)

performance; a reduction in speeds via increased $C_{L,max}$ can offer significant field length reduction at the low OEI power loading.

Blowing over the wing is also used for wing-borne cruise VTOL aircraft. Tilt-wing aircraft have been characterized as a 'hybrid' deflected slipstream VTOL because wing and flap are immersed in the propeller/rotor slipstream, historically with 2-4 propulsors. More recently, distributed propulsion enabled by hybrid/electric configurations has been proposed as a better method to control stall buffet and loss of lift in the transition corridor. Proposed configurations use distributed propulsors that are active for takeoff and landing and stowed during cruise ,[12,13] which fits well with the IHLP concept.

C. IHLP Impact on High Lift

The Integrated High Lift Propulsor considerably improves the effectiveness of DEP, resulting in a substantial reduction in thrust and power required and a significant improvement in cruise efficiency. This DEP performance benefit enables more efficient and economical hybrid and electric aircraft.

A brief overview of lift augmentation via blowing shows the challenges of DEP and opportunities of IHLP. For an infinitely large jet, the lift increase due to blowing is simply the increase in slipstream dynamic pressure. A slat trades better because the lift increment ΔC_L is now multiplied by the slipstream dynamic pressure ratio.

$$C_L = \left(\frac{V_j}{V_\infty}\right)^2 C_{L,unblown} \tag{2}$$

Combining Eq. 2 with momentum theory indicates that propeller diameter (area) should be minimized to minimize thrust (and power).

$$\left(\frac{V_j}{V_\infty}\right)^2 = 1 + \frac{T}{q_\infty A_p} \tag{3}$$

However, a finite jet does not fully achieve lift in proportion to slipstream dynamic pressure. A surrogate model developed by Patterson,[14] using inviscid 2D Computational Fluid Dynamics (CFD) for propeller locations typical of a pylon configuration, shows the actual lift augmentation peaks at a particular propeller diameter to chord (D/c) and falls off rapidly on the decreasing diameter side. This surrogate model trend is not universal, but a product of the chosen design. A similar model generated by Wayfarer using IHLP shows that the peak D/c is moved to significantly smaller propeller sizes, reducing the thrust required.

Viscous effects have a significant influence on the minimum effective slipstream size as well, causing separation due to adverse pressure recovery when the slipstream is not divided at the trailing edge.[15] The influence of propeller vertical position on separation was noted at least as early as NASA's 1960s VTOL research.[16] This viscous separation effect penalizes pylon mounted DEP that is typically mounted further ahead of the wing than IHLP, which increases the angle of attack sensitivity of the propeller slipstream position relative to the wing. The overall effect is that IHLP enables smaller propellers to be used more effectively, reducing the thrust and power required.

For electric motors, reducing propeller diameter has an additional benefit in reducing the total torque required. It is generally accepted that electric motor weight is more closely related to torque than power; for example, electric motor weight model in the NASA Design and Analysis of Rotorcraft (NDARC)[17] is reported as

$$W = 0.5663 * Q^{0.8207} \tag{4}$$

where W is the weight in lb and Q is the torque in ft-lb.

Many other literature sources give a similar relationship with slight variations in fit coefficients. The consequence of this torque dependent relationship is an additional motor matching benefit to smaller propellers; the all-else-equal effect of reducing propeller D/c from 1 to 0.375 is a 50% motor weight reduction. This torque-based sizing relationship also reduces the motor's physical dimensions, which is beneficial for IHLP packaging.

D. IHLP Impact on Cruise Efficiency

For DEP used to enable more efficient aircraft, the impact of nacelle drag with pylon mounted configurations is a substantial penalty. Recent studies oriented toward efficient 50 seat regional aircraft found that despite enabling a smaller, more cruise optimized wing, the nacelle drag resulted in DEP *increasing* total drag[15,18] in many cases, with the combination of small D/c and lower positions - seemingly optimal from the high lift standpoint - giving the worst net drag performance. Even when net drag was reduced, the nacelle drag reduced the maximum benefit by 60% compared to the wing alone. Similarly, the lower wing loading NASA X-57 reports that the high-lift nacelle drag is 9% of the total aircraft drag, which reduces the wing resizing benefit by about 25%. For comparison, this nacelle drag increment is roughly 1.5 times the reported drag increment between extensive laminar flow and a fully turbulent wing, or double the reported benefit of wing tip cruise motors.[19]

By stowing the propulsors internally, IHLP enables the high lift benefits of DEP without a cruise drag penalty. The all-else-equal tradeoff of reduced drag versus the additional mechanism weight for equal range and payload can be shown via the Breguet range equation, an idealized approximation of mission performance that gives a compact and technology level agnostic result. The constant weight electric Breguet range equation[20] used here differs slightly from the traditional consumed fuel versions, but the results are representative for either case as the improved aerodynamic efficiency (L/D term) is dominant. This analysis, presented in Fig. 4, shows that there are benefits for virtually all aircraft, which become increasingly large for cruise optimized regional aircraft.

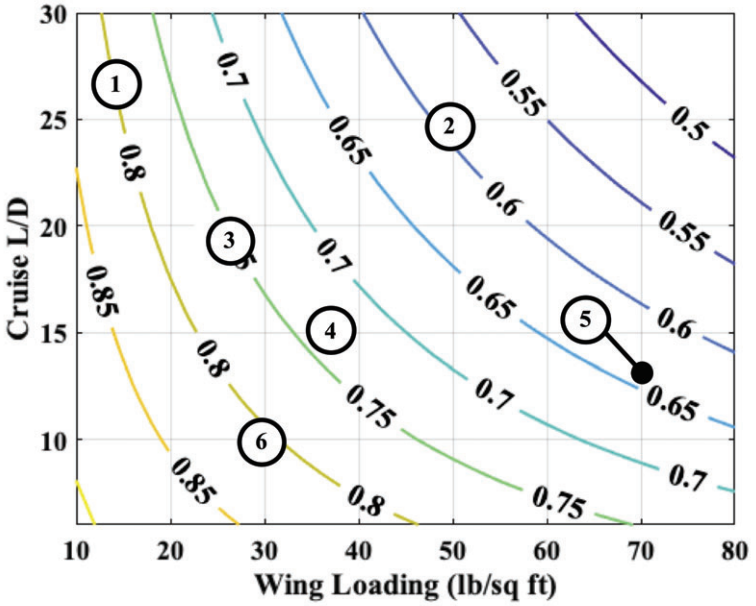

1. Pipistrel Taurus 4 — 3 Pax
2. MQ-9 UAV — 5600 lb UL
3. GA Mojave UAV — 3600 lb UL
4. Pilatus PC-12 — 9 Pax
5. ATR-42-500 — 48 Pax
6. Tecnam P2012 — 11 Pax

Figure 4. All-else-equal energy use of IHLP compared to Pylon DEP.

E. Summary

The net effect of blown wing aerodynamics and electric motor characteristics is illustrated in a comparison to the X-57 configuration in Fig. 5. While this aircraft used pylon DEP with folding propellers inactive in cruise, the results are equally applicable to configurations that use DEP for both high lift and cruise. With all else equal, the IHLP enables more than twice the number of propulsors, at lower overall power, to be effectively employed (table in Fig. 5). The reduced power and propeller diameter reduces torque and distributes it across more propulsors, enabling the motor integration with the slat. The overall result is a 25% reduction in high lift power required and a 35% increase in cruise efficiency.

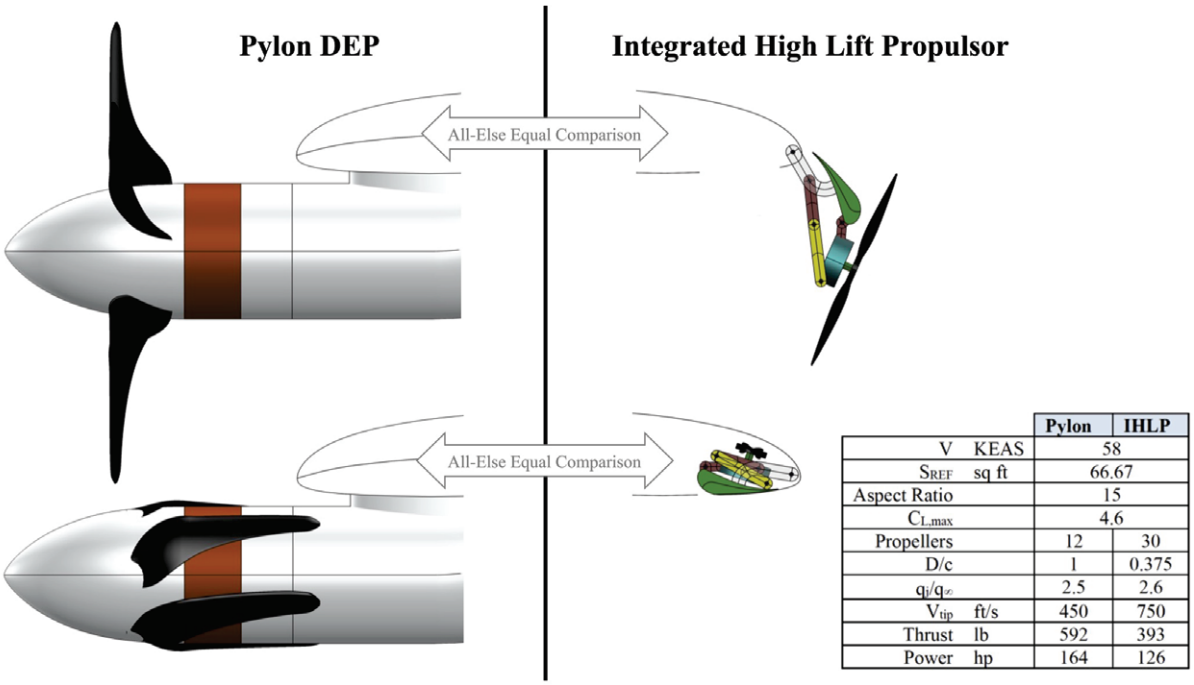

		Pylon	IHLP
V	KEAS	58	
S_{REF}	sq ft	66.67	
Aspect Ratio		15	
$C_{L,max}$		4.6	
Propellers		12	30
D/c		1	0.375
q_j/q_∞		2.5	2.6
V_{tip}	ft/s	450	750
Thrust	lb	592	393
Power	hp	164	126

Figure 5. Integrated High Lift Propulsor compared to Pylon DEP.

III. Subscale Aircraft

A. Introduction

This section provides an overview of the design and modifications of the 35%-scale Cessna 182 (C-182) to create the IHLP research aircraft, which is shown in Fig. 6. The C-182 was chosen as a well-known aircraft representative of potential IHLP design constraints, particularly for a retrofit or derivative wing design. Originally designed in the 1950s, the Cessna 182 is still in production today with over 20,000 aircraft built. The wing is a conventional strut-braced all-metal design using the 12% thick NACA 2412 with a single slotted flap. The slat chord and leading-edge volume are constrained by the forward spar at 15% (Fig. 1). This wing geometry has been extensively studied previously using CFD and experimentally in the Mississippi State University low speed wind tunnel.[10] The Eagle Flight Research Center at Embry-Riddle Aeronautical University operates an instrumented Cessna 182, which will be flown in a limited flight research campaign to gather validation data for the subscale aircraft in the baseline configuration.

B. IHLP Modifications

The Integrated High Lift Propulsor performance is a function of both traditional Krueger flap/slat and DEP design parameters; the parameters are presented in Fig. 7. The quasi-2D influence of these parameters has been studied

Figure 6. Modified 35% C-182 Subscale Research Aircraft.

extensively using CFD and validated experimentally,[10] nonetheless it was expected that the subscale flight test program would result in additional configuration refinement. In addition, the optimal configuration is likely to vary with aircraft design and mission objectives. For these reasons, the research aircraft IHLP modifications were designed to maximize configuration flexibility, which necessitated fixed (non-retractable) slat and motors.

The baseline aircraft wing was modified by cutting out the lower leading edge wing skin to create the coves into which the slat and motor retract on an operational system. These open coves are aerodynamically representative and enabled access to the interior of the already-manufactured wing to install the motor and slat mounting structure. The IHLP motor batteries are also installed through the open coves, mounting to brackets attached to the main spar as is shown in Fig. 8. The motor mount structure consists of a c-channel track mounted to a new forward spar. The slat brackets are attached to the same track at fixed locations.

The c-channel track permits the DEP motor mounts to be installed anywhere along the span of the wing, allowing variations in the size and number of propellers and the spacing between propellers. The DEP motors, which are correct physical scale, are capable of powering COTS propellers from 8" to 16" diameter (D/c $0.36-0.72$), limited by motor RPM and torque limits respectively. To accommodate all possible spanwise locations, including in-line with wing ribs or slat brackets, offset motor mounts were designed where the center of the propeller is laterally offset inboard or outboard from the center of the wing interface. The motor mounts are designed to vary tilt around the center of the propeller at a fixed $(x/c, z/c)$ location relative to the wing leading edge, which is shown in Fig. 9. The propeller $(x/c, z/c)$ position relative to the leading edge is varied by selecting different holes in the motor mount tube.

The slat installation consists of inboard and outboard carbon fiber panels attached to the wing with brackets interfacing to the same c-channel track as the motor mounts. The slat bracket design allows varying slat angle at fixed gap and overlap. The slat gap and overlap is not field adjustable, but can be varied by interchanging one low-cost laser cut slat bracket part shown in Fig. 10.

To return to the baseline Cessna 182 configuration the motor mounts and slat brackets are removed and the cove cutouts are covered with fairings. Conversion between the baseline and IHLP configuration or between different IHLP configurations can be completed in less than one day, enabling efficient testing of the influence of IHLP parameter variations on Performance and Handling Qualities (P&HQ).

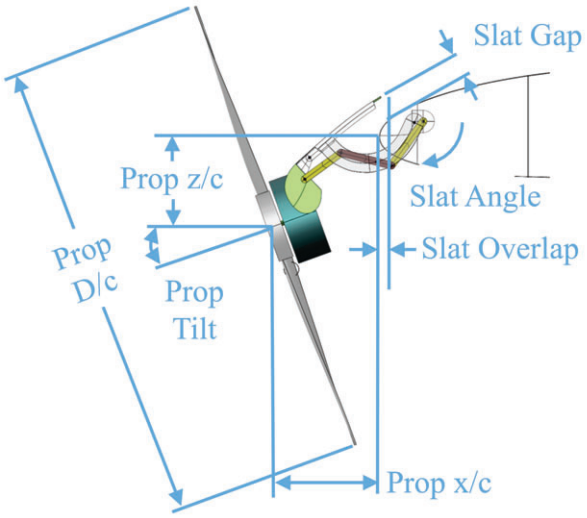

Figure 7. Integrated High Lift Propulsor parameters.

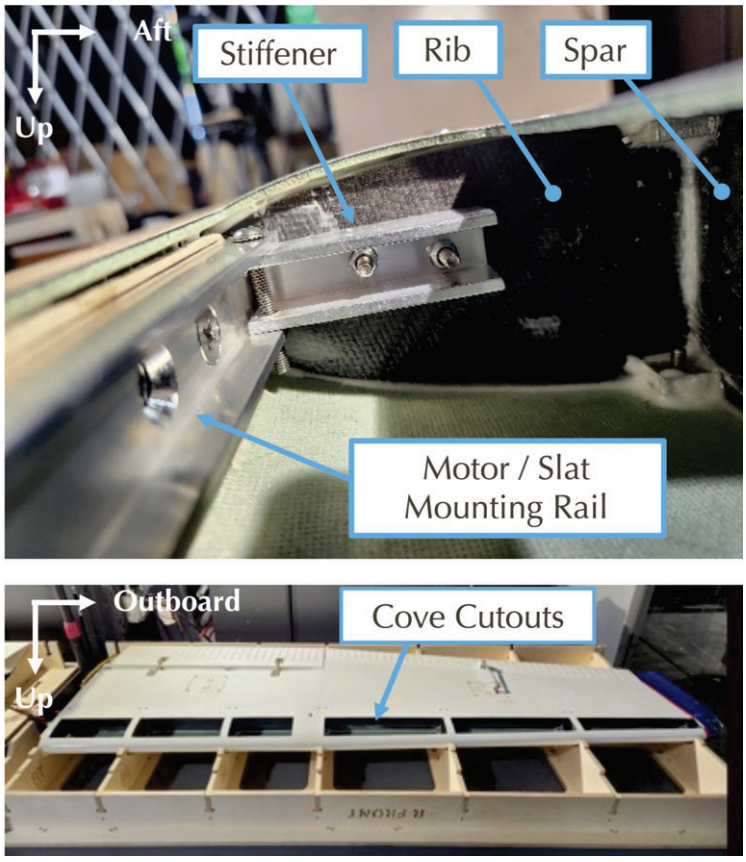

Figure 8. Wing modifications for the Integrated High Lift Propulsor.

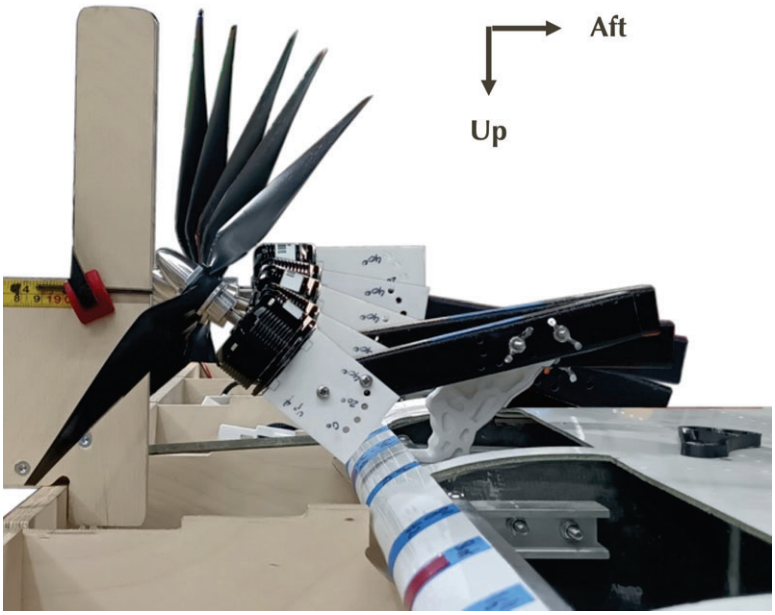

Figure 9. Motor Mount Tilt Capability.

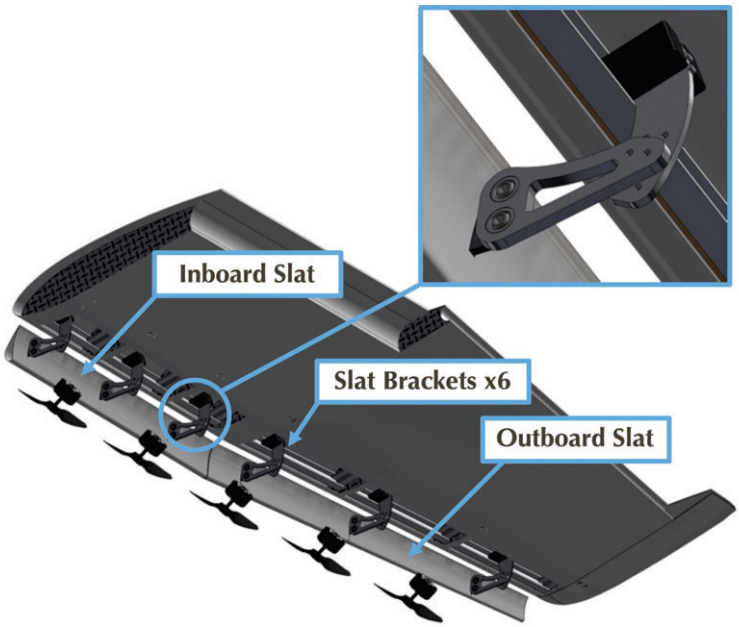

Figure 10. Slat Installation.

IV. Instrumentation Design Aspects

Instrumentation of the IHLP reconfigurable distributed electric propulsion subscale testbed presented many unique design aspects not previously encountered on other subscale and unmanned aircraft. The process to develop an adequate platform starts with understanding the underlying problem: what type of data needs to be collected. This could often involves performing an extensive study of platforms currently available as well as those that have been developed at universities and research agencies. In the course of this study, individuals at various institutions may also surveyed. This research then leads to an extensive list of desired specifications, most often based on what is state of the art. The first and likely most critical consideration that must be taken into account is that of the intended uses of a platform and the sensors required. Essentially, what data must be captured and why? On the type of aircraft this paper focuses on, this list would likely include measurements from inertial, global positioning (GPS), analog, actuation (servo PWM), ported air-data, and propulsion sensors (commanded throttle, power, RPM).[21–23] The IHLP testbed presents a challenge in instrumention design with a large number of measurements directed.

The next consideration is that of platform integration, i.e., how will it be integrated into the aircraft and therefore, if there are size, weight, access constraints. This is especially important on unmanned aircraft, which leads to the notion that a platform must likely be highly integrated; however, at the same time, such tight integration can be restrictive, especially if modifications must be made. Should the platform designer, for example, split the data acquisition between multiple logical devices, sending all of the measurements back into a central device. This could be advantageous in distributing the work, especially if some logical devices can be given the task of handling high-level tasks while others handle low-level tasks. Yet implementing such a platform design may lead to sensory streams having undesirable temporal properties, which in turns affects the quality of produced data. Alternately, the platform be made up of a single logical device prudently managing all of the sensors and measurement devices. Generally, performing benchmark testing of a platform will help determine which approach should be used.

After development of the data acquisition system, there lies the the challenge of integrating a flight controller into the instrumentation system. Specifically, the primary challenge lies in ensuring the flight controller and its supporting software are robust, accurate, and capable of managing the complex demands of operating an aircraft. This aircraft requires precise and fast translation of pilot inputs into physical responses, alongside additional functionality such as data acquisition, integration with the primary data acquisition system, and execution of programmed maneuvers autonomously. In addition, the system must coordinate inputs from multiple sources, including the pilot, onboard sensors, and external systems, to make real-time decisions and control various components such as control surfaces, electric propulsors, and the primary motor. Addressing these requirements demands a reliable and advanced flight control platform capable of handling high-speed data processing and extensive input/output operations. This process is outlined in Fig. 11

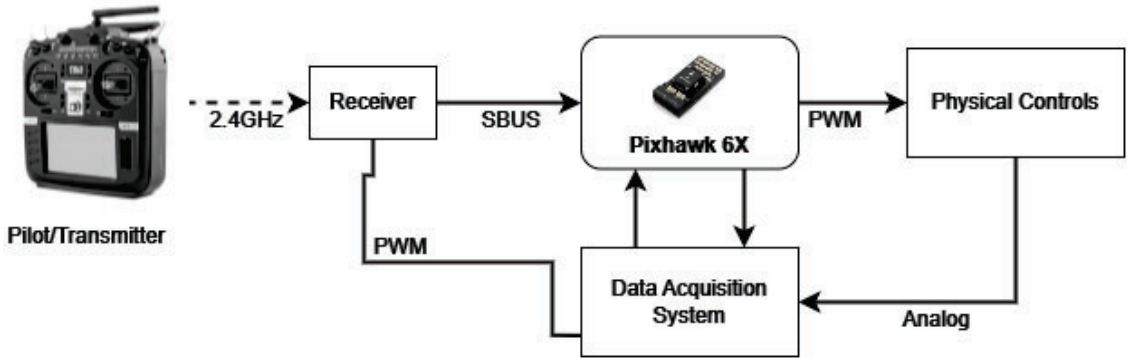

Figure 11. A preliminary system diagram for the subscale model.

In order to reach design maturity, testing is key. Initial development is often performed by piecing together and interconnecting a set of mostly independent, integrated circuit (IC) components, each on their own printed circuit board (PCB). The strict segregation of components is initially used to test each and every subsystem individually,

while designing the software/hardware infrastructure with the integration goal in mind. The *divide et impera* approach has shown to produce highly reliable sensor-processor communication. Then, as the system is miniaturized, these components moved into close proximity with each other. Apart from the obvious hardware integration, subtle signal interplay and similar issues arising from circuit-level integration must be extensively investigated and addressed. Many issues are largely software dependent, as timing properties of software-hardware interaction routines need to be re-calibrated once all the subsystems are contemporarily active. For other issues, new revision of the hardware layout are often required and yield the most reliable solution in terms of reliability and robustness. Flight testing, throughout the whole miniaturization process also reveals several other challenges that cannot be discovered on the ground. These challenges along with the methods used to overcome them will be highlighted.

Minimizing the time required to develop and integrate a platform into an aircraft is also very important and thus a crucial design driver that must be taken into account. Effectively, there is little point to perform system development if the end results will either be too late to meet a project timeline or be impossible to integrate. Therefore, significant effort should be put into developing a self-contained system that could be assembled, installed, and controlled. Regarding control, the end use researcher must be able to interface with the platform in order to communicate required commands. This can mean a wired or wireless connection; however, extra care should be taken with the later for some applications, especially those with possible RF interference or other limitations. Thus, the goal of this particular design effort is to ensure that in a complex environment, as most aircraft testing setups are, the platform can be self-contained, not cause interference, and finally be controllable. Effectively, this describes the deployability of the platform solution, which is especially difficult on highly-integrated, electric unmanned aircraft such as the IHLP subscale testbed aircraft.

V. Development

The development of the IHLP reconfigurable distributed electric propulsion subscale testbed instrumentation included both a custom data acquisition system and a custom flight control system. These two efforts were performed simultaneously at Al Volo LLC and Embry Riddle Aeronautical University's Eagle Flight Research Center, respectively, and then integrated into the subscale testbed by Wayfarer Aircraft.

A. Data Acquisition System Development

The development of the IHLP testbed data acquisition system included many challenges. Challenges included the integration of sensors that had not been previous integrated in Al Volo products; for example, interfacing with and retrieving propulsion system data from an APD electronic speed controller and pressure measurements from a Surrey Sensors Pressure Scanner (among many others). Additional challenges included the integration of a large number (12) of DEP propulsion system interfaces, i.e. via 12 Al Volo Castle Interfaces; which had not been done previously in such a high quantity. The large amounts of sensors and flight measurements desired also created the challenge of fusing and logging such large amounts of data.

The ambitious task of developing the custom data acquisition system for the IHLP subscale aircraft was therefore broken down into a several stages - individual sensor preliminary integration, multi-sensor prototype integration, and complete sensor integration. Fig. 12 shows an example of an individual sensor integration task, whereby the software to integrate with the APD ESC is being developed using a laptop computer. Later, Fig. 13 shows an example of a multi-sensor prototype integration where a load cell interface (measuring propeller thrust) is being tested, while optical RPM is being simultaneously measured, and 4 sets of Castle ESC propulsion data are being captured by 4 Al Volo Castle Interfaces. This led to the complete sensor integration of all the custom and standard Al Volo instrumentation, which is shown in Fig. 14; the complete specifications of the data acquisition system is presented in Table 1 in the next section.

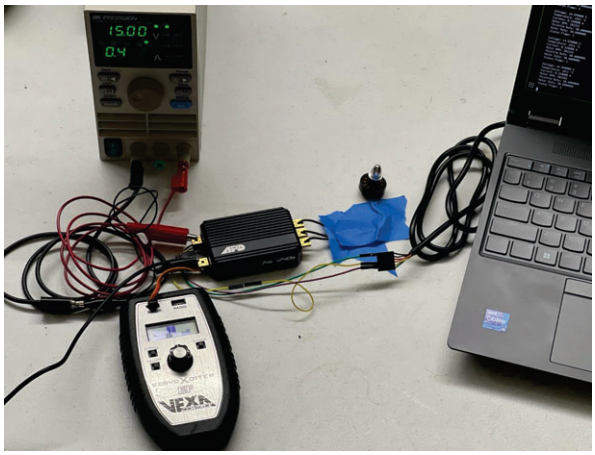

Figure 12. The preliminary integration of the APD ESC, being tested using a laptop computer.

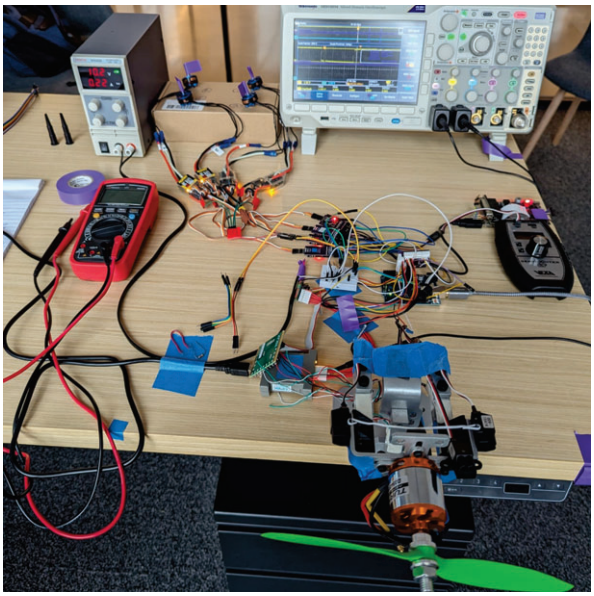

Figure 13. The under-development data acquisition portion of instrumentation

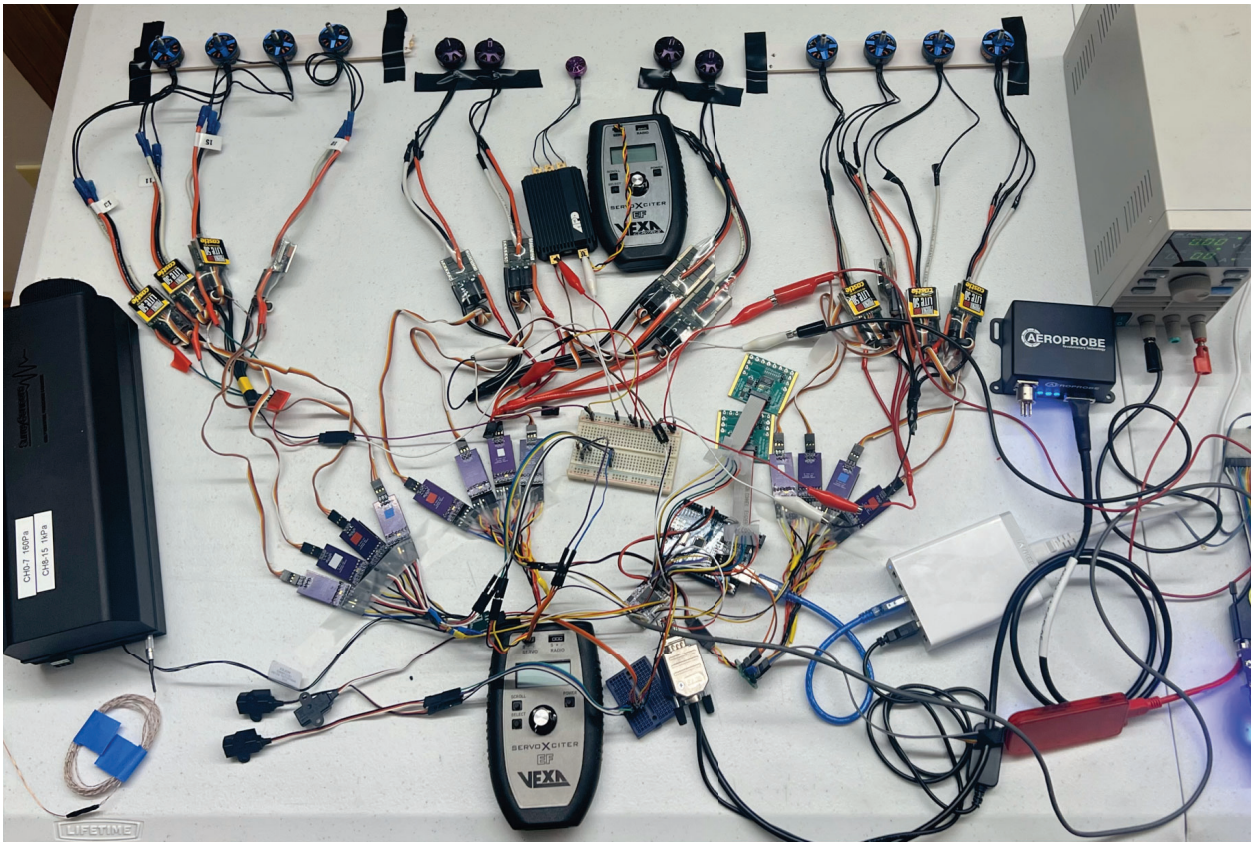

Figure 14. The complete testbench data acquisition portion of the custom Al Volo instrumentation with 12+1 test motors, to simulate 12 IHLP motors and 1 main motor.

B. Flight Control System Development

The flight control system was developed from a Pixhawk 6X flight controller. The PX4 firmware was supplemented with custom flight control software written in MathWorks Simulink using the UAV Toolbox Support Package for PX4 Autopilots.[24] This software allows maneuvers to be injected precisely and consistently into the aircraft for the purposes of parameter identification. In addition, limited autopilot capability is available for test efficiency and in the event of lost link to the transmitter. The aircraft has three flight modes: manual, damped, and maneuver injection, which are shown in Fig. 15. Manual flight mode directly passes the PWM signals from the transmitter into the PWM channels of the main motor and control surfaces. Damped mode adds a value to the commanded control surface deflection angle that was based on the measured angular rates, this acts as a damper that could reject small disturbances in flight. Finally, maneuver injection mode allows for a set of predetermined instructions to be executed on the aircraft.

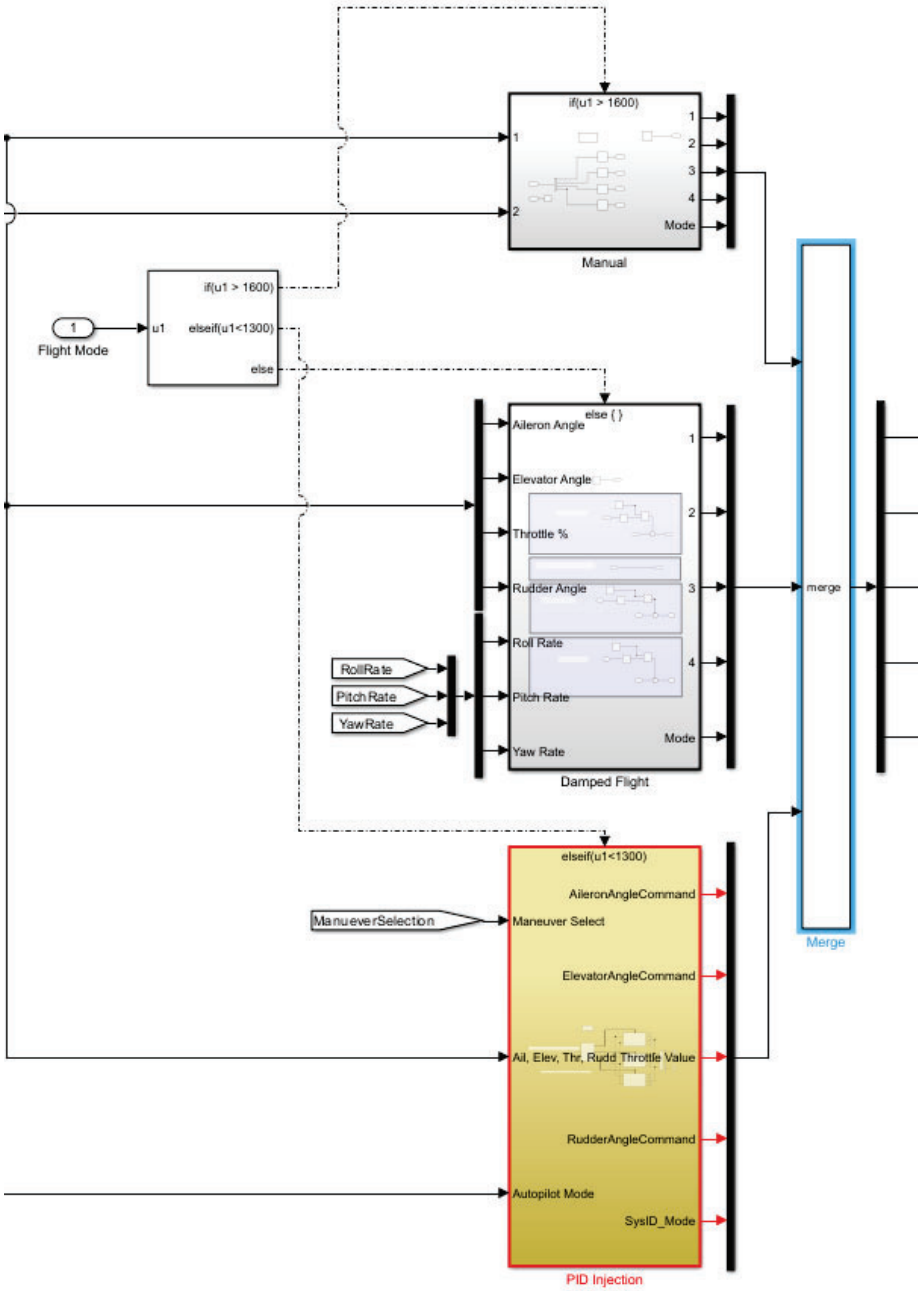

Figure 15. A screenshot of the mode selection code in Simulink

VI. Aircraft Instrumentation

A. Introduction

This section will provide a description of the integration of the instrumentation and flight control system into the aircraft. Many of the components have been attached to a single instrumentation rack that can be removed for maintenance and are located within the fuselage of the aircraft with access provided through either of the main cabin doors (Fig. 16). Design constraints require specific sensors and controllers to be in different locations which will be discussed later in this section. Components were sized and selected based on project parameters and are presented in Table. 1. Power is provided to the instrumentation and flight control system through a series of Li-Po batteries, as is shown in Fig. 17. One 3S 11.1V 2200 mAh battery supplies the components of the data acquisition, motion sensing, air data collection, and interface systems, while two 2S 7.4V batteries provide completely redundant power sources for the flight controls.

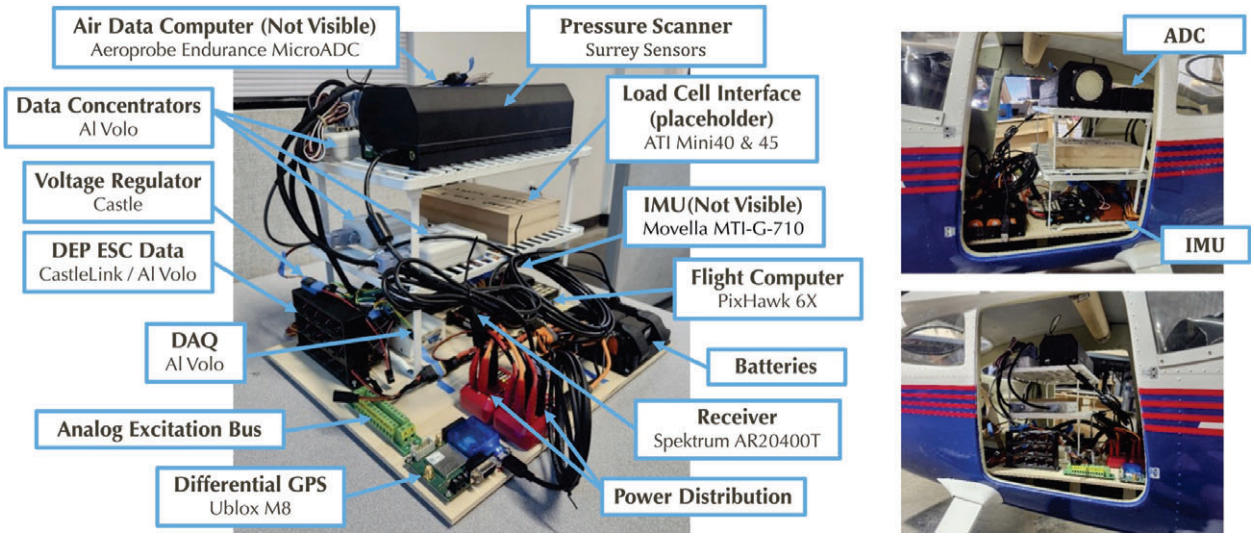

Figure 16. The IHLP testbed subscale aircraft instrumentation rack.

B. Component Description

At the center of the instrumentation system are the PixHawk 6X Flight controller and the custom Al Volo FDAQ. Both components are located on the main level of the instrumentation rack within the fuselage allowing for shorter and more centralized connection points between these components and the sensors and flight controls they command and monitor. The Pixhawk accommodates several connections including an S-bus adapter input, RSSI outputs, and a UART serial data connection between itself and the FDAQ. It also contains an onboard IMU, and connects to a GPS antenna and RF telemetry antenna, allowing for real-time monitoring of the aircraft flight conditions through the Mission Planner App. The FDAQ and its expansion boards receive and manage data from many sources, including PWM signals from all flight control surfaces, analog signals from all flight control position sensors, motion data from an external IMU, differential GPS time and location data, 6 axis force/moment inputs from two load cells, pressure and air data from two air data booms and main and DEP motor ESC parameters; a diagram is presented in Fig. 18. It also houses an internal memory for data log storage and can telemeter data over RF to a ground station, allowing for real-time data visualization and monitoring the state of the aircraft in flight.

The motion of the aircraft is monitored by a XSens MTi-G-710 AHRS IMU with GNSS and the position is tracked by the uBlox NEO-M8P Differential GPS (DGPS) and its associated ground station antenna, allowing for GPS correction and providing centimeter location accuracy. Both GNSS antennas as well as the PixHawk GPS antenna are located on the cockpit glareshield, allowing for clear line of sight to the sky, while the RF antenna that provides GPS corrections is located on the belly of the aircraft; the antennas are presented in Figs. 19 and 20. Both the IMU and DGPS are located on the main instrument rack and transmit data to the FDAQ via a USB and serial port connection respectively.

Table 1. Instrumentation Sensors.

Flight Controller	Holybro Pixhawk 6X
Data Acquisition System	Custom Al Volo FDAQ 100 Hz
Motion	
Inertial Measurement Unit	XSens MTi-G-710 AHRS with GNSS
Positioning System	uBlox NEO-M8P RTK GNSS with basestation
Air Data	
Air Data System	AeroProbe Endurance micro air data computer
Air Data Boom	AeroProbe 5-Hole probe
Wake Survey System	Surrey Sensors Pressure Scanner and AeroProbe 5-Hole probe
Propulsion	
Main Motor Sensor	(1x) APD HV ESC interface
Main Propeller Thrust & Torque	(1x) ATI Mini45 6-axis Load Cell with (1x) Al Volo Load Cell Interface
Main Propeller RPM	(1x) Al Volo Optical RPM sensor
IHLP Motor Sensors	(12x) Al Volo Castle ESC interface
IHLP Propeller Thrust & Torque	(1x) ATI Mini45 6-axis Load Cell with (1x) Al Volo Load Cell Interface
IHLP Propeller RPM	(2x) Al Volo Optical RPM sensors
Flight Controls	
Servo Commands	(8x) PWM Channels
Control Position	(8x) TT Electronics Hall Effect sensors
System Modes	(8x) PWM channels & (TBDx) Control Law parameters
Interface	
Data Downlink	900 MHz serial radio
Onboard	UART serial interface
Configuration	Wifi-based interface

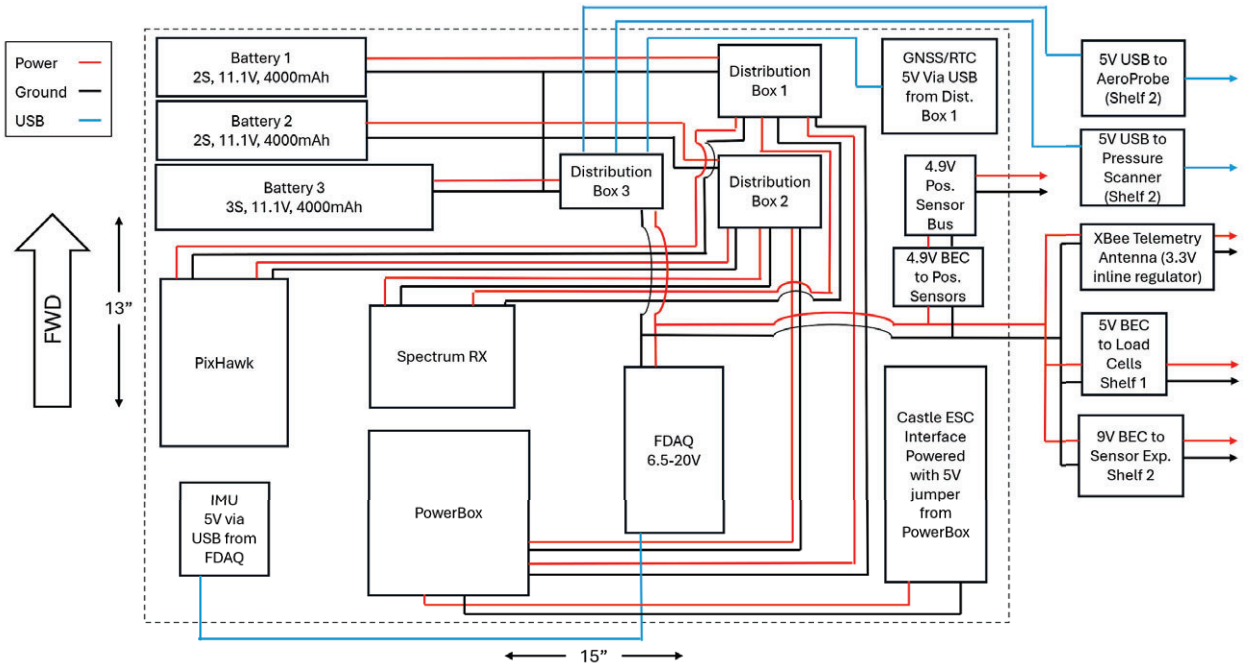

Figure 17. Power distribution wiring diagram.

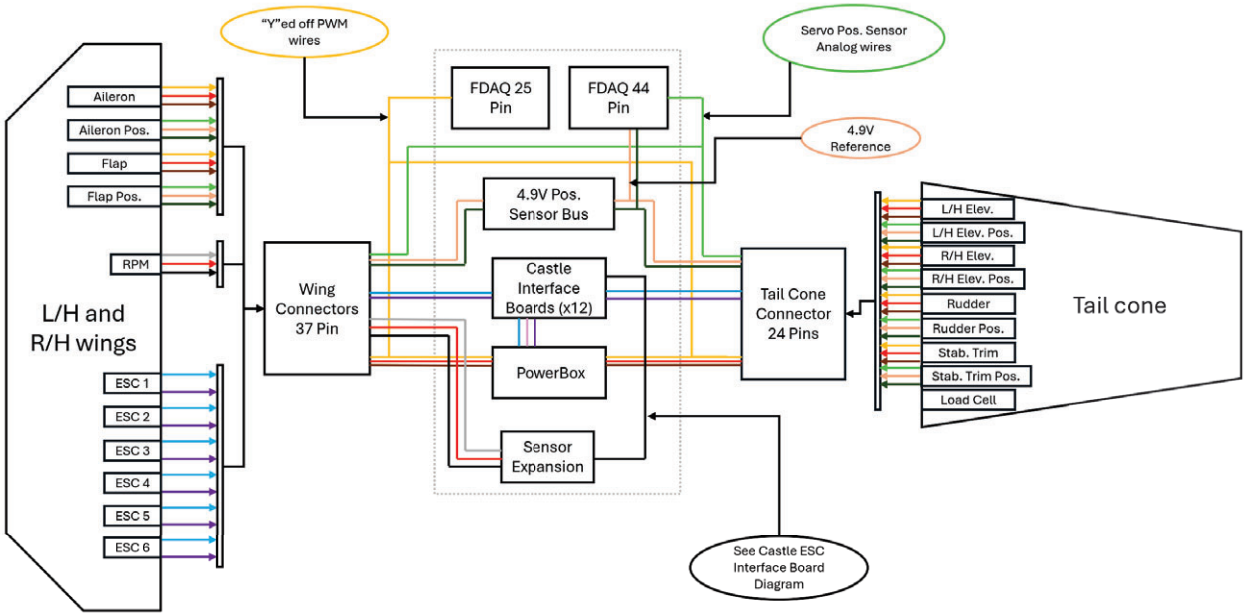

Figure 18. FDAQ wiring diagram.

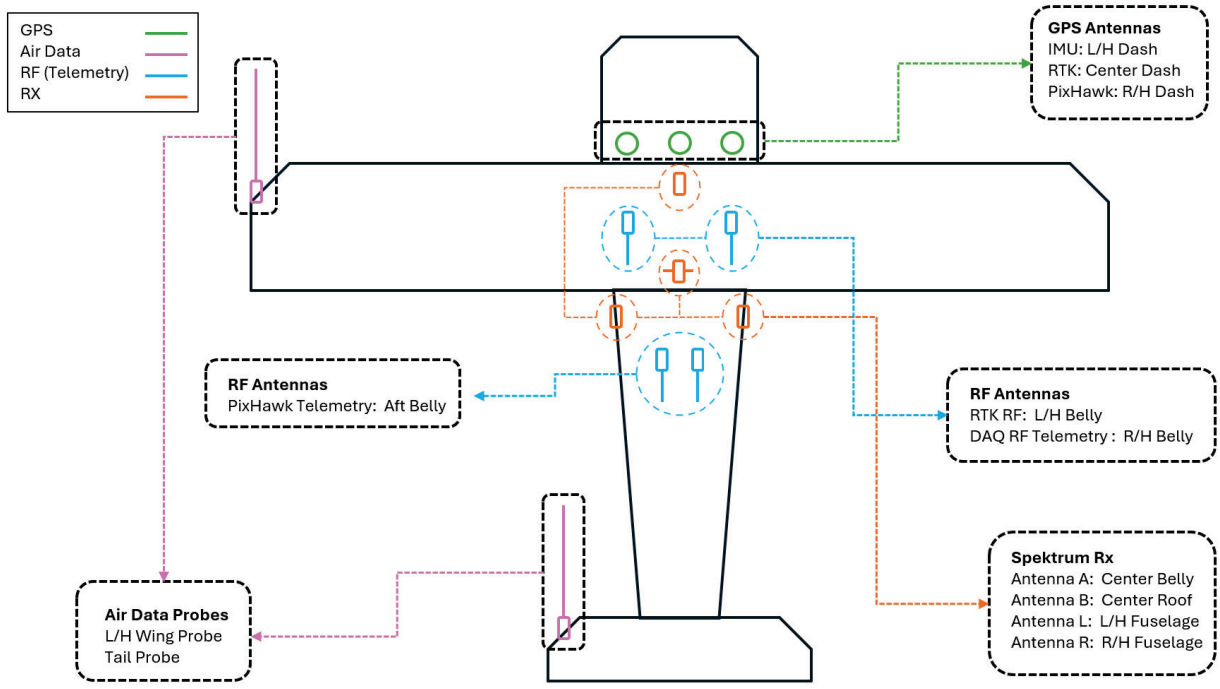

Figure 19. Aircraft antenna and probe layout.

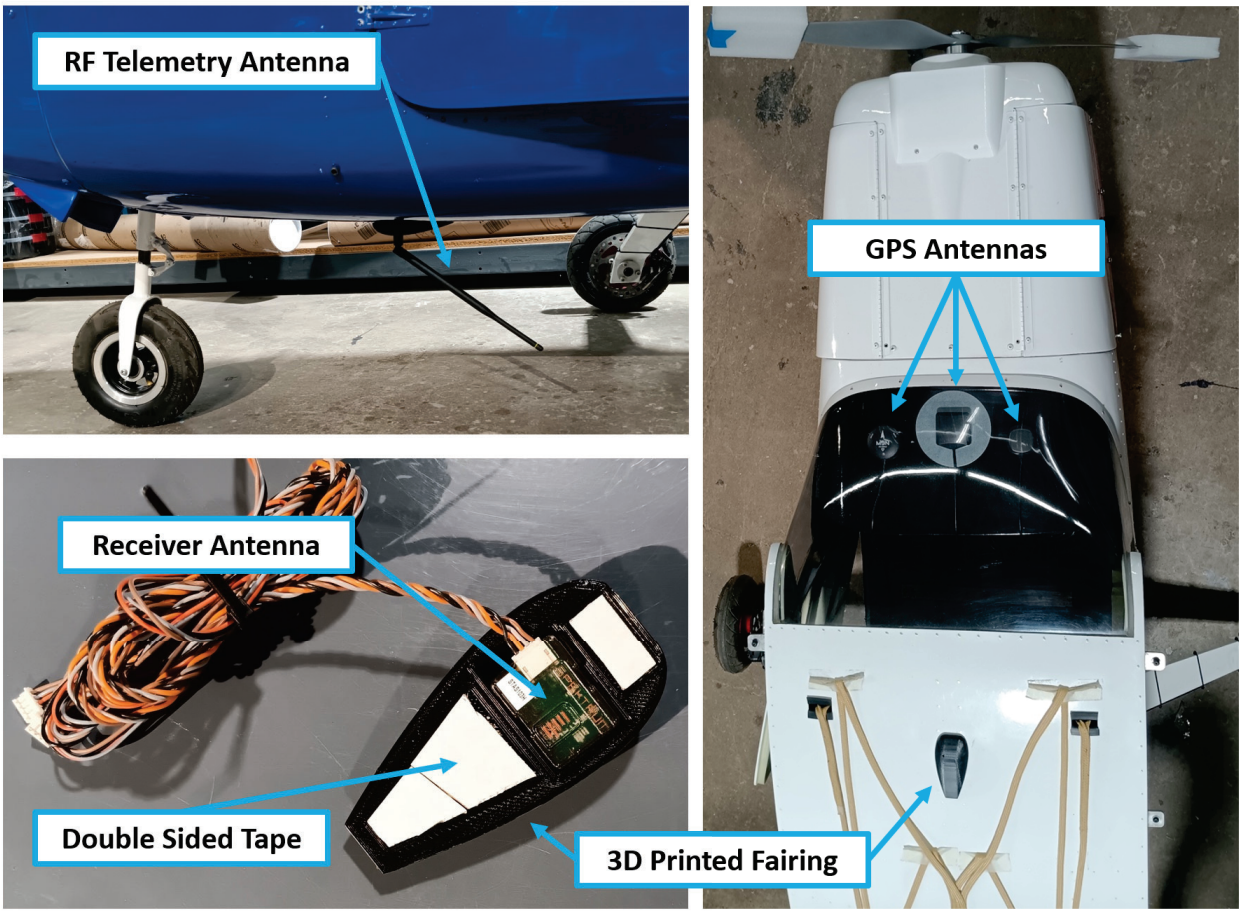

Figure 20. Aircraft antenna locations.

Wing and tail booms are used to sense pressure data to determine that aircraft flight condition. A boom connected to the left-hand wing that is shown in Fig. 21 houses an AeroProbe 5-Hole probe which transmits pressure data to the AeroProbe Endurance Micro Air Data Computer (μADC). The μADC uses a 2" H_2O range focused on low-speed and high-AoA accuracy and incorporates wind-tunnel probe calibrations to ± 40 α and β at 20 and 60 knots. The corrected air data is then fed to the FDAQ over a serial bus. Another boom and 5-hole probe are connected to the left-hand horizontal stabilizer for wake survey, as shown in Fig. 21. The horizontal stabilizer is in both the wing downwash and main propeller slipstream, with flow conditions strongly influenced by main propeller thrust. The wake survey probe enables characterization of these influences, which strongly affect longitudinal stability and trim. The wake survey 5-hole probe is plumbed to the Surrey pressure scanner 1 kPa differential pressure transducers. The tail probe static pressure is measured differentially from the wing air data boom absolute static pressure measurement. This data is again fed to the FDAQ over a serial connection. The recorded raw pressure data is post-processed to apply the wind tunnel calibration and extract α, β, static and dynamic pressure at the tail.

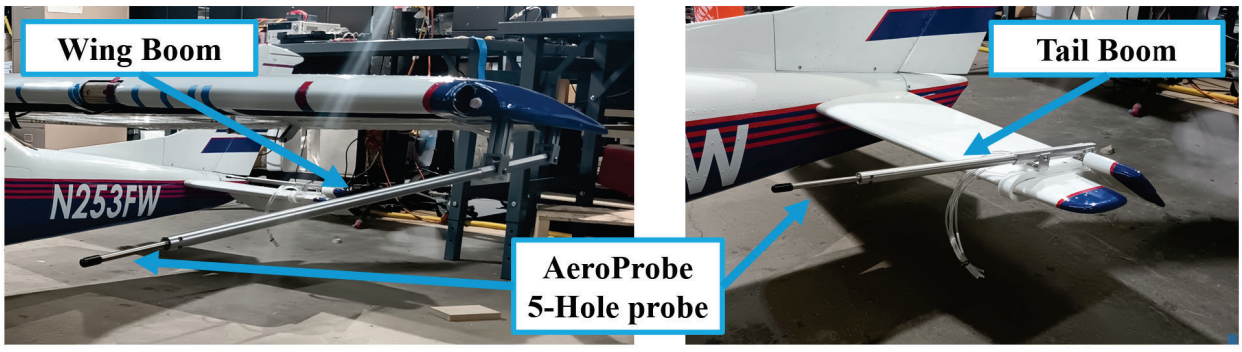

Figure 21. Air data booms and probes.

The flight control system is made up of a Spektrum IX-20 transmitter, Spektrum AR20400T receiver, Powerbox Competition SR2 power distribution, MKS HV777A+ servos, and TT Electronics Hall Effect position sensors; a diagram is presented in Fig. 22. The receiver features 4 seperate antennas for redundancy, housed within external 3D printed teardrop fairings with each antenna oriented in a different plane (Fig. 20). In normal manual operation mode the pilot gives commands to the aircraft through the transmitter and receiver. The primary flight control inputs are sent to the Pixhawk via a S-Bus adapter and then passed through via RSSI to the Powerbox. From here, power and PWM signals are sent to the flight control servos and raw PWM signals are also sent back to the FDAQ for monitoring. Connected to each servo is a TT Electronics Hall Effect sensor that produces a voltage between 0 and 5 volts depending on the position of the servo arm; an example is shown in Fig. 23. This analog voltage signal is sent back to the FDAQ for monitoring. The pilot is also capable of selecting an auto pilot mode in which the PixHawk commands predetermined maneuver injections. The flight control system also contains a rescue parachute that can be deployed at any time by the pilot or by the PixHawk in the event of a persistent loss of link.

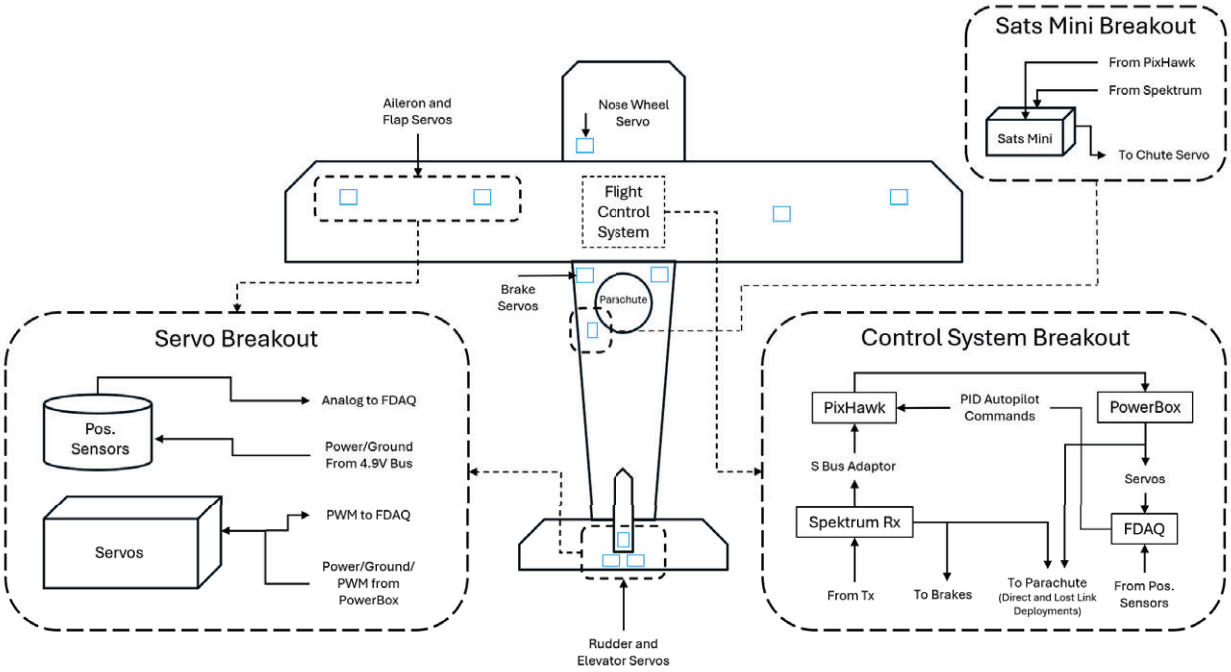

Figure 22. Flight control system layout.

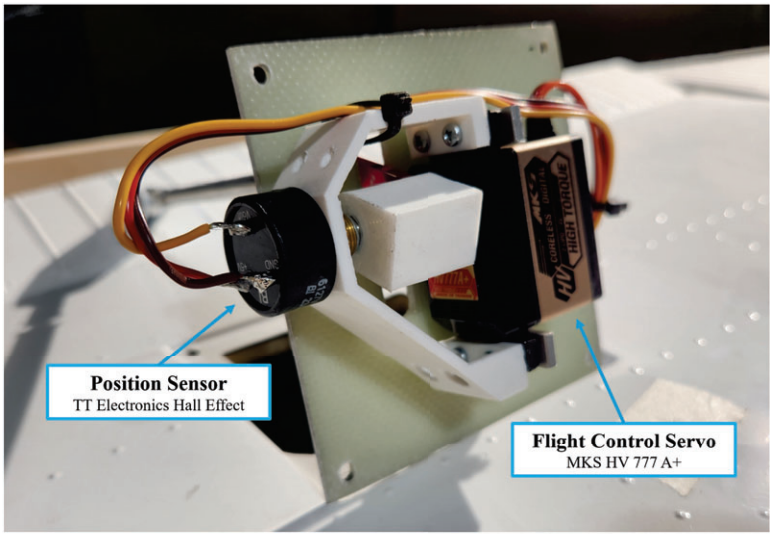

Figure 23. Flight control servos and position sensors.

The aircraft propulsion consists of two separate systems, main and DEP, as can be seen in Fig. 24. The main system consists of the Neumotor 12030/174 electric motor, two 12S 44.4V 12,000 mAh batteries in parallel, the APD HV ESC, and an optical RPM sensor, while the DEP system consists of up to 12 DEP Neumotor 3814/7.5/438 electric motors, their associated 12S 44.4V 2,000 mAh batteries, Castle Phoenix Edge HV ESC's, Castle ESC Interface boards and two optical RPM sensors. The pilot commands both systems via transmitter inputs in the same way as the flight control inputs (this is explained in more detail in subsection C). However, in this case the Powerbox sends signals to the motors through individual ESCs. The main ESC is located in the nose section, DEP ESCs are attached to the DEP motor mounts. The location of the ESCs is driven by the proximity requirement to the batteries, as long leads can cause AC disturbances and power losses. The respective ESCs are powered directly by their associated motor battery. The main motor parameters are sent directly from the APD ESC to the FDAQ over UART serial connection for monitoring. For the DEP system the motor parameters are first passed through the Castle ESC Interface boards (Fig. 25) for processing using CastleLink protocol before being sent to the FDAQ.

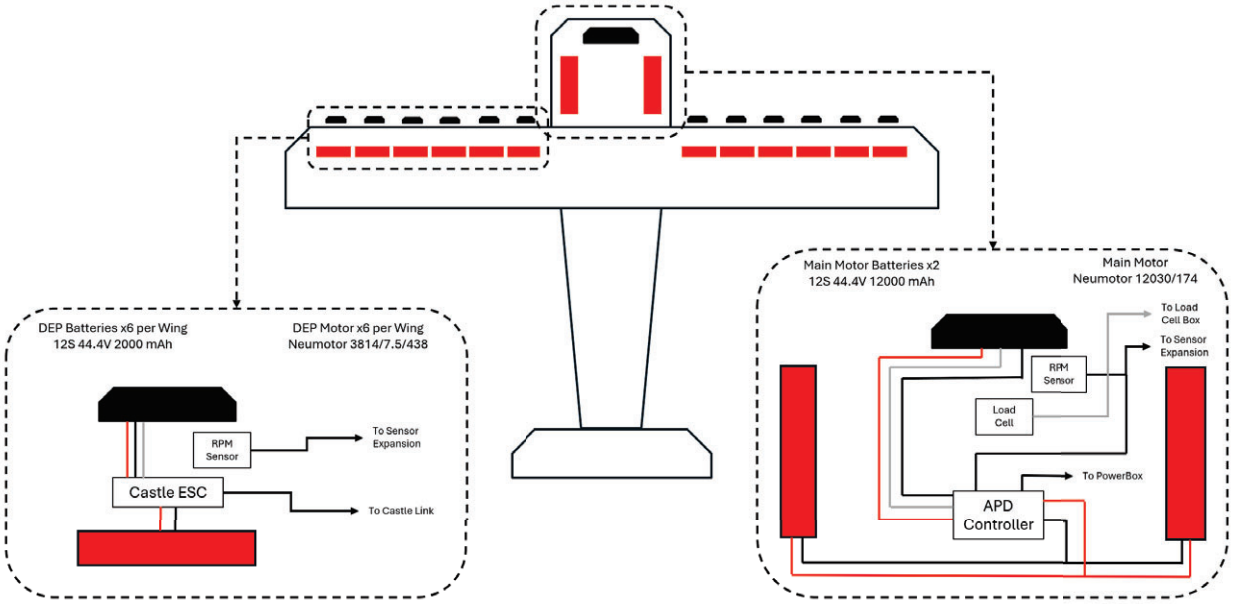

Figure 24. Aircraft propulsion system.

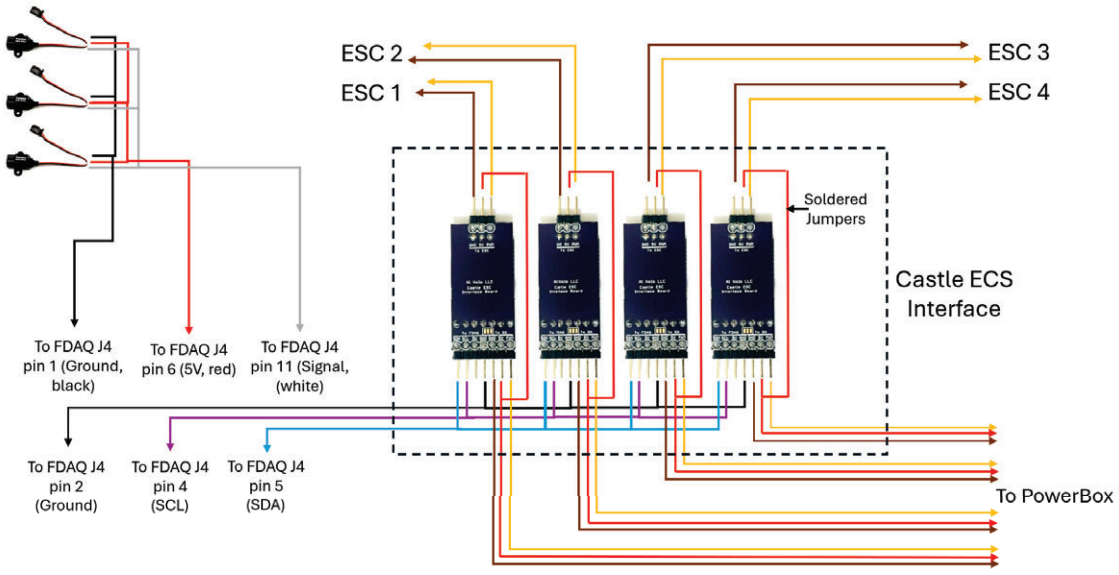

Figure 25. Al Volo Castle Interface board wiring diagram.

C. Ground Station

Data from both the PixHawk and FDAQ are telemetered to a laptop ground station. The PixHawk data is telemetered to the ground station laptop using the RFDesign RFD 900x telemetry system and displayed using the ArduPilot Mission Planner.[25] The custom parameters from the SimuLink model are not currently available over telemetery, but may be added in the future. Since the aircraft controls are not conventionally interfaced with the PixHawk, the primary purpose of the PixHawk telemetry is situational awareness using the moving map and GPS/IMU derived Primary Flight Display, which are presented in Fig. 26.

Figure 26. An example of ArduPilot Mission Planner.[25]

The FDAQ data is telemetered to the laptop ground station using a pair of Digi XBee-Prop XSC S3B Long-Range Modules. The FDAQ interface allows the serial data stream sample rate and parameter list to be configured as desired. The baseline setup transmits 188 parameters, which is almost the entire set of logged data from all sensors (Table 1); a few parameters that are not relevant in real time are omitted. This data set is well within the 14 KB/s bandwidth of the 115200 8N1 baudrate serial stream. Custom Matlab functions parse the serial stream messages and apply conversions to engineering units, calibrations, and computations of derived parameters in real time. The processed data is then passed to plotting functions that update each ground station screen display or plot. The ground station screen is arranged in tabs that group the data displayed by function, such as the propulsion system, as shown in Fig. 27. To improve the update rate, only the active tab displays are updated. Additional displays for overall Situational Awareness (SA) are constantly displayed in a left hand panel (not shown). In addition to preset displays, a generic strip chart tab is included with plots that can be interactively configured to display any available parameters.

At the time of writing, the FDAQ ground station development is ongoing to add additional plots and displays required for flight. The laptop ground station displays are relatively simple, intended primarily for additional SA during testing versus the real-time data analysis capability of more complex ground stations. Nonetheless, it has already proved invaluable for real-time troubleshooting and development.

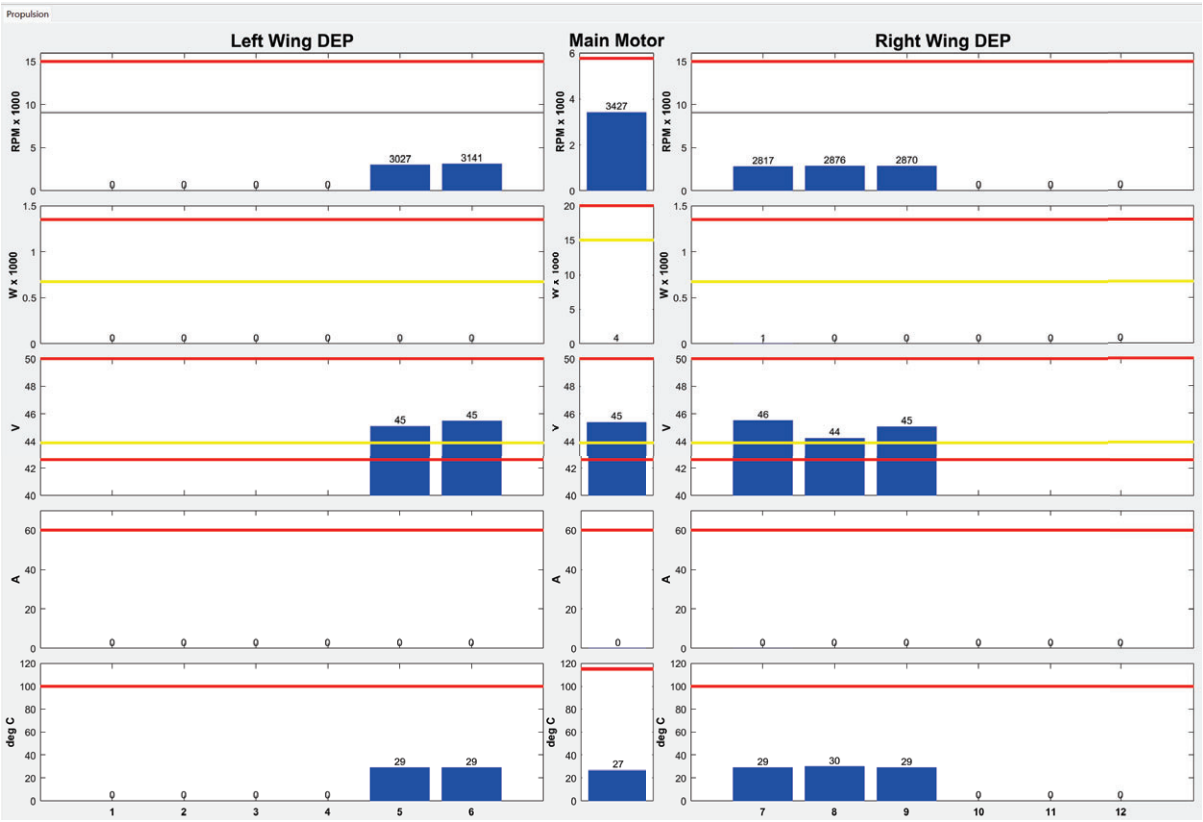

Figure 27. FDAQ ground station propulsion screen

VII. Flight Control

A. Flight Control Hardware

The primary components of the flight control system are a Spektrum IX-20 transmitter, Spektrum AR20400T receiver, Holybro Pixhawk 6X flight computer, and Powerbox Competition SR2 power distribution box. In addition, the Fruity Chutes SATS-MINI self-contained IMU[26] is used to control the parachute deployment, including automatic deployment in the event of loss of control following lost link. The flight control schematic is presented in Fig. 28.

The Pixhawk 6X controls servos that actuate the control surfaces, and sends commands to the IHLP motors and the main motor. Hardware limitations meant that only 10 of the 20 receiver channels could be input to the PixHawk. This problem was solved by bypassing the PixHawk for channels that did not require maneuver injection, such as the wheel brakes, and by using the FDAQ to pass through additional PTI mode selection channels over UART to the PixHawk (Table 2), which then deciphered the serial data into PWM commands that it could process, effectively extending the maximum number of input channels.

The Pixhawk also supplements the primary data acquisition system by logging its own set of parameters to an onboard SD card that can combined with FDAQ data in post-process. The FDAQ sends a counter that increments on each sample over UART to the PixHawk. The simultaneous logging of the same signal on both systems enables post-flight time synchronization of the independently logged data.

B. Flight Control Software

The flight control software has been broken down into 4 subsections: control inputs, sensors, data logging, and control outputs.

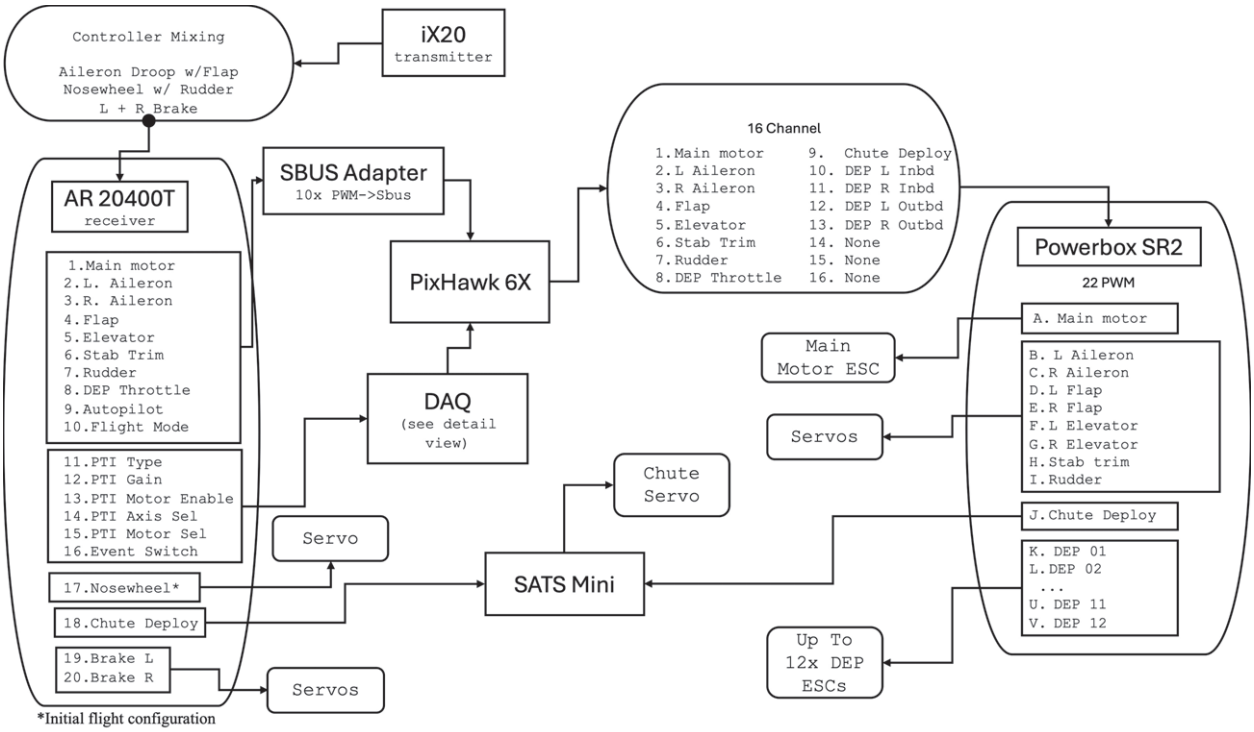

Figure 28. Aircraft flight control schematic.

The control inputs subsection is responsible for taking the inputs from the receiver, as well as the additional inputs from the data acquisition system, and converting them into control surface angles that the rest of the software can process. It is also responsible for selecting which flight mode the aircraft should be in and the parameters for the maneuver injection.

The sensors subsection processes the raw outputs from the GPS, inertial measurement unit, and onboard barometer to determine altitude, relative bearing, accelerations (linear and angular), and the orientation of the aircraft. This data is then passed through to the data logging section.

The control outputs subsection takes the control surface deflection angles determined by the flight control logic and converts them back into PWM values that can be passed through to the Pixhawk. In addition to that, it is responsible for handling the lost-link logic in the event the transmitter and receiver become disconnected.

Finally, the data logging subsection takes in all of the information from every other subsection, and logs it to a uLog topic stored to the SD card. These uLog topics can be read using MATLAB's built in uLog reading tools for further analysis and comparison to the data from the primary data acquisition system.

C. Pilot Interface

The aircraft is flown by the remote pilot using a Spektrum IX20 20- channel RC transmitter shown in Fig. 29 with functions listed in Table 2. The primary flight controls are a conventional fixed-wing configuration, with the addition of a separate DEP throttle and emergency parachute. The aileron droop mode switch controls whether the ailerons droop with flap deployment. Although the original full-scale Cessna 182 does not use drooping ailerons, it is available as an aftermarket STC modification.[27]

Additional transmitter controls allow the pilot to select the autopilot mode and control the PTI manuever type. The type of input (e.g. 3-2-1-1, Chirp, or Multisine) is selected with the PTI type switch. Subset groups of effectors are selected for maneuver injection using the PTI Motor Enable, PTI Axis Select, and PTI Motor Select switches. This is expected to be used primarily for test / maneuver development with most data collected using the multisine PTI input with all effectors active. The momentary Event Switch allows the pilot to mark the recorded data for any purpose.

Table 2. Functionality of Transmitter Controls.

Rx Ch	UART Ch	Functionality	Modes	Control
1		Main Motor Throttle	N/A	Left Control Stick ⇳
2		Left Aileron	Droop w/ Flaps on/off	Right Control Stick ⇔ Switch D2: Droop Enable
3		Right Aileron	Droop w/ Flaps on/off	Right Control Stick ⇔ Switch D2: Droop Enable
4		Flap	Up, Takeoff, Land	Switch D
5		Elevator	N/A	Right Control Stick ⇳
6		Stab Trim	N/A	N/A, Future Capability
7		Rudder	N/A	Left Control Stick ⇔
8		DEP Throttle	N/A	Right Rear Lever
9		A/P Mode	Off, Get Trim, Altitude Hold	Switch B
10		Flight Mode	Manual, Damped, PTI Inject	Switch C
11	1	PTI Type	3-2-1-1, Chirp, Multisine	Switch G
12	2	PTI Gain	Continuously Adjustable	Right Knob
13	3	PTI Motor Enable	PTI Motor Inputs On/Off	Switch E2
14	4	PTI Axis Select	Longitudinal, Lat/Dir, Both	Switch E
15	5	PTI Motor Select	Main, DEP, Both	Switch F
16	6	Event Switch	Mark Data, on/off	Switch I
17		Nosewheel	N/A	Left Control Stick ⇔
18		Chute Deploy	Fire command on/off	Switch H
19		Left Brake	N/A	Left Rear Lever
20		Right Brake	N/A	Right Rear Lever

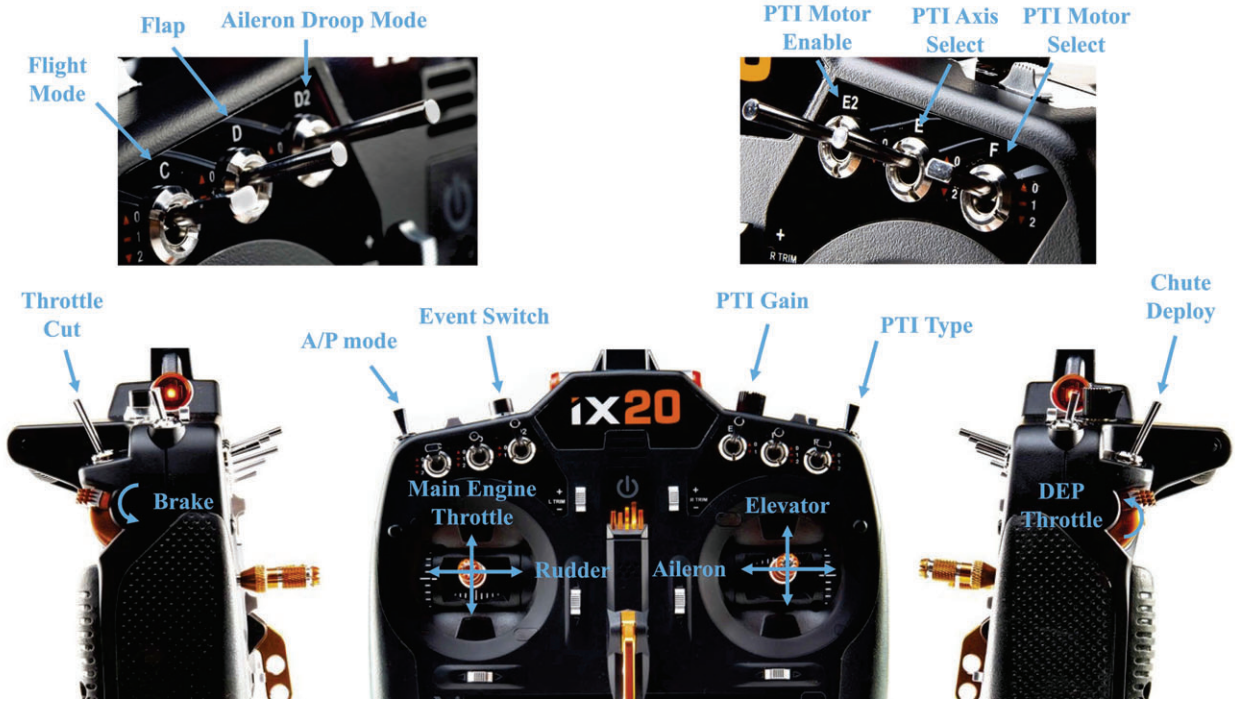

Figure 29. Layout of transmitter controls.

VIII. Initial Ground Testing Results

After completion of aircraft wiring harnesses and instrumentation rack (Fig. 16), validation testing of the instrumentation system commenced with a bench test setup (Fig. 30) that could exercise and end-to-end check the complete integrated system with all aircraft flight components, sensors, and wire harnesses. The wing and tail cannon plug disconnects allowed sensors in the wings and tail to be connected to the bench test setup before full aircraft installation / assembly. The bench testing has been sucessfully completed with all sensors end-to-end functionally checked.

In addition to individual sensor testing, calibration, and validation the instrumentation system has been used for static ground testing of the main motor at varying power levels. Full duration main motor runs at throttle settings ranging from 50% to full throttle have been completed, which will be used for flight planning and to set limitations. The static test rig and results from a 70% throttle full duration motor run is shown in Figure 31. The FDAQ telemetry allowed real-time monitoring of critical parameters and limitations such as main motor battery voltage and ESC temperatures during this testing, as well as ride-along functional testing of other parts of the instrumentation and flight control system. DEP motor testing has also been completed up to full power with bench mounted 3D printed prototype motor mounts. Additional runs at varying power will be completed with the final carbon fiber and aluminum motor mounts installed in the wing. Validation and verification of the autopilot and Programmed Test Inputs (PTI) for Parameter Identification (PID) are ongoing. Upcoming ground testing using the instrumentation system includes measurement of the full aircraft moments of inertia, validation of the lost-link autopilot logic, and bandwidth characterization of the motors and servos in preparation for the first flight.

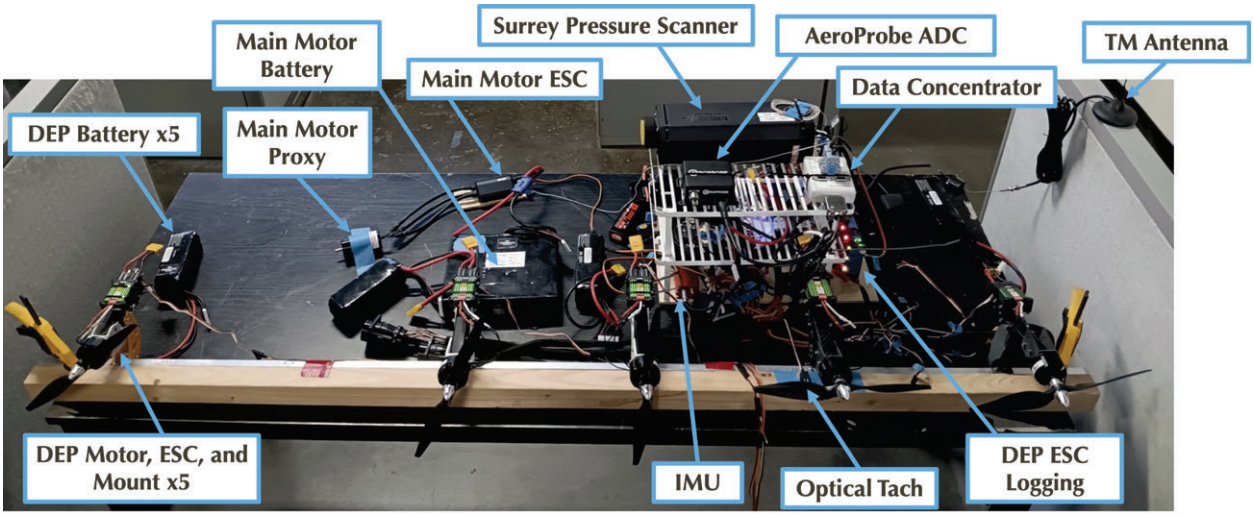

Figure 30. Instrumentation system bench testing.

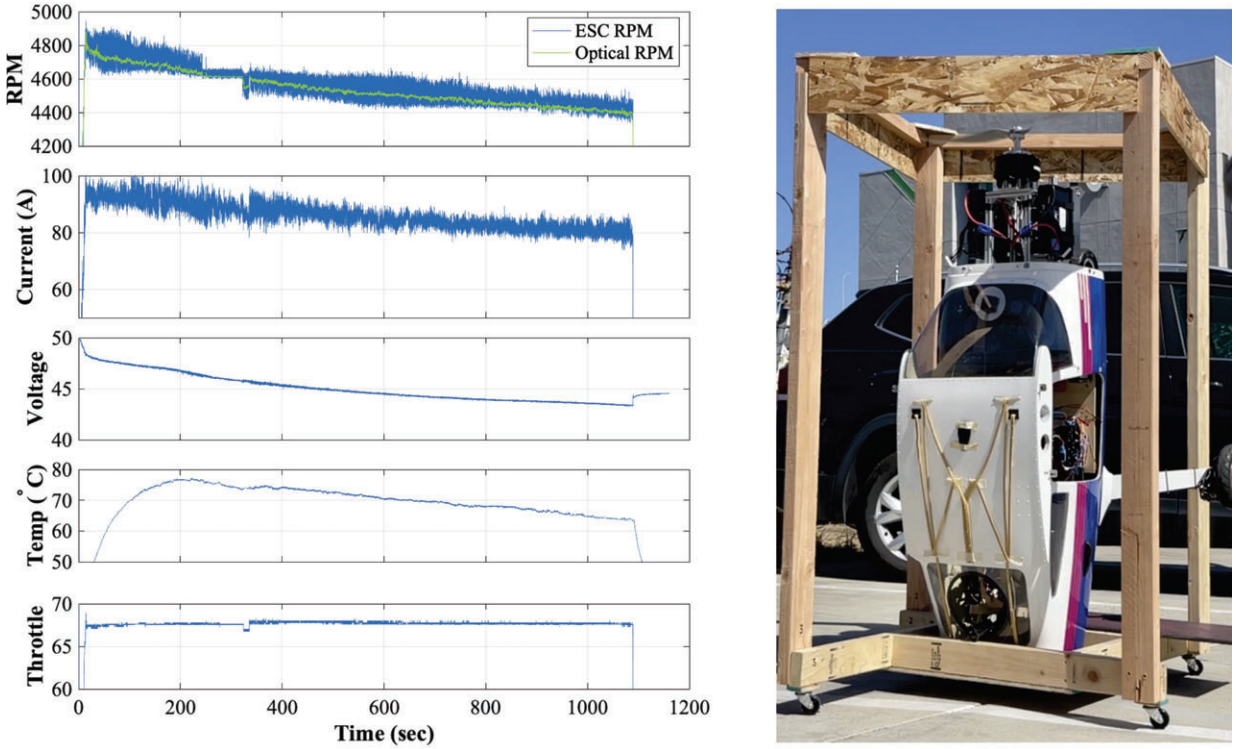

Figure 31. Main motor static testing.

IX. Summary and Future Work

This paper presented the instrumentation of a reconfigurable subscale IHLP distributed electric propulsion testbed, which was developed from a 35%-scale Cessna 182 R/C scale model aircraft. The subscale aircraft was instrumented with a custom-integrated flight control and data acquisition system developed to enable this flight research — specifically a Holybro Pixhawk 6X autopilot running custom flight control software coupled with a custom version of the Al Volo FDAQ data acquisition system. The paper presented IHLP including its advantages and performance improvements in high-lift and cruise conditions compared to conventional distributed electric propulsion (DEP) systems. The details of the development of the IHLP subscale testbed were presented, including modifications, instrumentation design, and the integration of the data acquisition and flight control systems. Preliminary results from ground testing were presented to demonstrate the capabilities of the IHLP testbed.

Completion of the final IHLP modifications and preparation of the aircraft for flight continues to support the first flight in early 2025. The aircraft will first fly in the baseline (without IHLP) configuration. System identification of the baseline will ensure that the incremental effects of the IHLP modification on P&HQ are correctly attributed and comparable to full-scale Cessna 182 P&HQ from flight testing of the Eagle Flight Research Center's full-scale instrumented Cessna 182. After completion of the baseline testing, the subscale aircraft will then begin progressive envelope expansion with the IHLP system in the initial configuration selected from CFD analysis to identify the blown wing P&HQ characteristics, which will be compared to preflight predictions. The effects of IHLP configuration variations such as propeller diameter, location, and tilt on performance will then be characterized. The flight test results and comparisons to preflight predictions will be published in a future paper.

Acknowledgments

Funding for this research was provided under NASA Phase II STTR contract 80NSSC24CA038. The authors would also like to thank Dr. Benjamin M. Simmons at NASA Langley for his advice and guidance during development of the flight control system maneuver injection capability.

References

[1]Borer, N., Patterson, M., Viken, J., Moore, M., Clarke, S., Redifer, M., Christie, R., Stoll, A., Dubois, A., and Bevirt., J., "Design and Performance of the NASA SCEPTOR Distributed Electric Propulsion Flight Demonstrator," Tech. Rep. NF1676L-22882, National Aeronautics and Space Administration, 2016.

[2]Ramirez, L., Decroix, J., Justin, P., A., C., and Mavris, D., "Design and Operation Considerations for the Integration of Fleets of Regional Air Mobility at Large Hubs," AIAA Paper 2021-3178, AIAA Aviation Forum, Virtual Forum, 2021.

[3]"Aura Aero," https://aura-aero.com, 2023.

[4]"EcoPulse," https://www.airbus.com/en/innovation/low-carbon-aviation/hybrid-and-electric-flight/ecopulse, 2023.

[5]"Electra," https://Electra.aero, 2023.

[6]McSwain, R., Geuther, S., Howland, G., Patterson, M., Whiteside, S., North, D., Glaab, L., and Rhew, R., "An Experimental Approach to a Rapid Propulsion and Aeronautics Concepts Testbed," Tech. Rep. TM-2020-220437, National Aeronautics and Space Administration, 2020.

[7]W. Fredericks, M. M. and Busan, R., "Benefits of Hybrid-Electric Propulsion to Achieve 4x Increase in Cruise Efficiency for a VTOL Aircraft," AIAA Paper 2013-4324, AIAA Aviation Forum, Los Angeles, CA, 2013.

[8]"Odys Aviation," https://www.odysaviation.com, 2023.

[9]"Regent," https://regentcraft, 2023.

[10]Ward, B., Deters, R. W., and Narsipur, S., "Experimental Analysis of the Integrated High-Lift Propulsor," AIAA Paper 2024-1508, AIAA SciTech Forum, Orlando, FL, 2024.

[11]Langelaan, J., Chakrabarty, A., Deng, A., Miles, K., Plevnik, V., Tomazic, J., Tomazic, T., and Veble, G., "Green Flight Challenge: Aircraft Design and Flight Planning for Extreme Fuel Efficiency," *Journal of Aircraft*, Vol. 50, No. 3, 2013, pp. 832–846.

[12]McSwain, R., Geuther, S., Howland, G., Patterson, M., Whiteside, S., North, D., Glaab, L., and Rhew, R., "An Experimental Approach to a Rapid Propulsion and Aeronautics Concepts Testbed," NASA/TM-2020-220437, 2020.

[13]Fredericks, W., Moore, M., and Busan, R., "Benefits of Hybrid-Electric Propulsion to Achieve 4x Increase in Cruise Efficiency for a VTOL Aircraft," AIAA Paper 2012-4324, 2012.

[14]Patterson, M.D., "Conceptual Design of High-Lift Propeller Systems for Small Electric Aircraft," Ph.D. Dissertation, Department of Aerospace Engineering, Georgia Institute of Technology, Atlanta, Georgia, 2016.

[15]Hawkswell, G., Miller, R., , and Pullan, G., "election of Propeller-Wing Configuration for Blown Wing Aircraft," AIAA Paper 2022-1024, 2022.

[16]Hassell, J. and Kirby, R., "Descent Capability of Two-Propeller Tilt-Wing Configurations," Conference on V/STOL and STOL Aircraft, AMES Research Center, April 4-5, 1966, NASA SP-116, 1966.

[17]Whiteside, S. K. S., Pollard, B. P., Antcliff, K. R., Zawodny, N. S., Fei, X., Silva, C., and Medina, G. L., "Design of a Tiltwing Concept Vehicle for Urban Air Mobility," NASA TM 20210017971, 2021.

[18]Barry, M., Maury, C., and Turnbull, T., "Aerodynamic evaluation of distributed propulsion for a regional aircraft," AIAA 2023-3393. AIAA Aviation Forum, June 2023, 2023.

[19]Deere, K., Viken, J., Viken, S., Carter, M., Wiese, M., and Farr, N., "Computational Analysis of a Wing Designed for the X-57 Distributed Electric Propulsion Aircraft," Nasa NF1676L-25695, 2017.

[20]de Vries, R. and Hoogreef, M.F.M. and Vos, R., "Range Equation for Hybrid-Electric Aircraft with Constant Power Split," *Journal of Aircraft*, Vol. 57, No. 3, 2020, pp. 552–557.

[21]Mancuso, R., Dantsker, O. D., Caccamo, M., and Selig, M. S., "A Low-Power Architecture for High Frequency Sensor Acquisition in Many-DOF UAVs," International Conference on Cyber-Physical Systems, Berlin, Germany, Apr. 2014.

[22]Dantsker, O. D. and Mancuso, R., "Flight Data Acquisition Platform Development, Integration, and Operation on Small- to Medium-Sized Unmanned Aircraft," AIAA Paper 2019-1262, AIAA SciTech Forum, San Diego, California, Jan 2019.

[23]Dantsker, O. D. and Mancuso, R., "Propulsion System Instrumentation Development and Integration on Small-and Medium-Sized Electric Unmanned Aircraft," AIAA Paper 2022-2156, AIAA SciTech Forum, San Diego, California, Jan 2019.

[24]"UAV Toolbox Support Package for PX4 Autopilots," https://www.mathworks.com/help/uav/px4-spkg.html.

[25]"ArduPilot Mission Planner," https://ardupilot.org/planner/docs/mission-planner-overview.html.

[26]"SATS-MINI - Sentinel Automatic Trigger System," https://shop.fruitychutes.com/products/sats-mini-sentinel-automatic-trigger-system.

[27]"Robertson STOL High Lift Systems," https://skyway-mro.com/robertson-stol-high-lift-systems/.